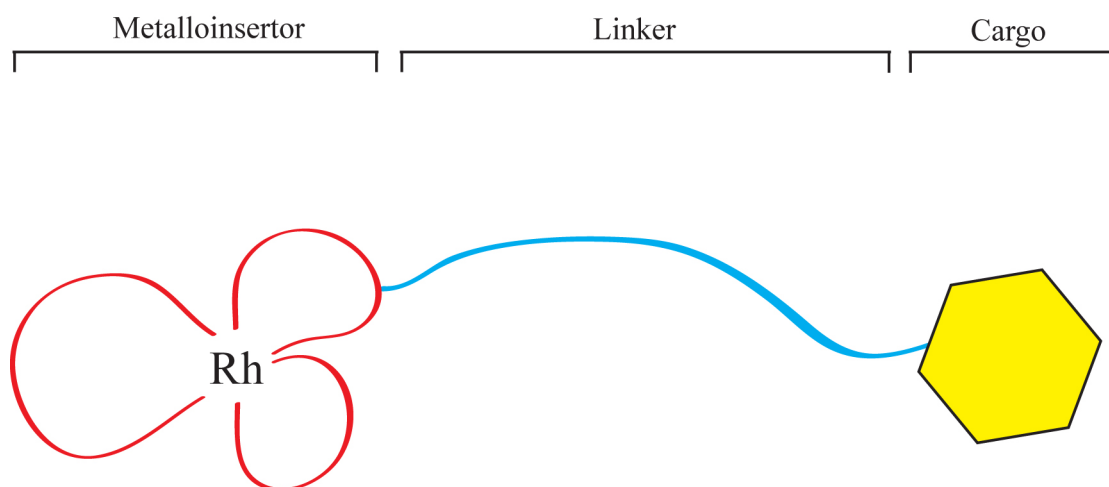


## CHAPTER 7: THE DESIGN AND SYNTHESIS OF MISMATCH-SPECIFIC BIFUNCTIONAL CONJUGATES

### 7.1: INTRODUCTION

The diagnostic and therapeutic potential of mismatch-specific metalloinsertors became evident very soon after their discovery. Therefore, over the past ten years, our laboratory has sought to develop these complexes for various clinical applications.<sup>1,2</sup> The first generations of metalloinsertors, most notably  $\text{Rh}(\text{bpy})_2(\text{chrysi})^{3+}$  and  $\text{Rh}(\text{bpy})_2(\text{phzi})^{3+}$ , have shown significant promise as agents for the detection of mismatches<sup>3,4</sup>, single nucleotide polymorphisms<sup>5</sup>, and abasic sites.<sup>6,7</sup> Furthermore, the ability of both these complexes, among others, to preferentially inhibit the proliferation of mismatch repair (MMR) deficient cells makes them attractive candidates for use as chemotherapeutics against MMR-related cancers.<sup>8,9</sup>

Yet the overall promise of metalloinsertors is not limited to that of the complexes alone. Indeed, these mismatch-specific agents can be employed in conjugates to confer site-specificity on useful but otherwise non-specific agents.<sup>10-14</sup> Structurally, these bifunctional conjugates must necessarily feature a tripartite design, with metalloinsertor, linker, and cargo subunits (**Figure 7.1**). The conjugates are assembled convergently. A linker-modified ligand is first synthesized and then metallated onto a pre-formed  $\text{Rh}(\text{phen})(\text{chrysi})(\text{NH}_3)_2^{3+}$  framework to yield the completed linker-modified, trisheteroleptic metalloinsertor (see Chapter 2 for details and synthetic schemes), for example  $\text{Rh}(\text{phen})(\text{chrysi})(^{\text{NH}_2}\text{bpy})^{3+}$ . This subunit is then covalently attached to the desired cargo via standard peptide coupling procedures. Importantly, the inherent

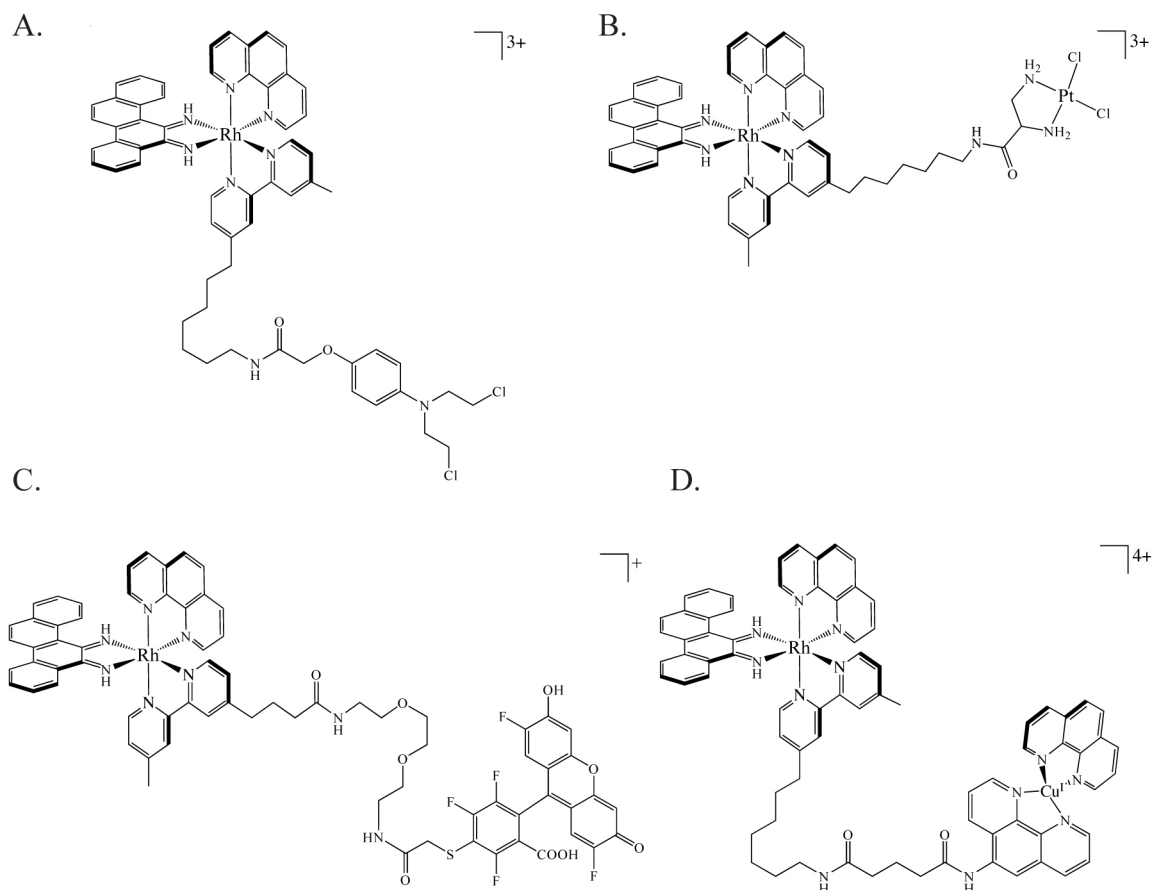


**Figure 7.1. The anatomy of a bifunctional conjugate.** The metalloinsertor subunit (red) is covalently tethered to the cargo moiety (yellow) by a flexible linker (blue).

modularity of metal complexes and the convergent synthetic approach to these conjugates affords the opportunity to exploit a variety of metalloinsertor, linker, and cargo moieties. To date, our laboratory has designed, synthesized, and tested bifunctional conjugates employing platination agents<sup>13</sup>, alkylators<sup>12</sup>, DNA-cleaving copper complexes<sup>11</sup>, fluorophores<sup>14</sup>, and cell-penetrating peptides<sup>10</sup> (**Figure 7.2**). All have enjoyed a measure of success. For example, the metalloinsertor subunit of the DNA alkylator conjugate (**Figure 7.2a**) is able to specifically direct its nitrogen mustard subunit to alkylate DNA near mismatched sites. Further, the metalloinsertor-Oregon Green conjugate discussed earlier in this text (**Figure 7.2c**, Chapter 3) successfully acts as a mismatch-specific fluorescent probe, if only as a proof of concept.

Yet despite these successes, the overall *in vitro* and *in vivo* applicability of the conjugates has remained limited. At fault are two disparate issues, likely acting in concert: poor cell permeability and reduced DNA binding affinity. The former, while outside the scope of this chapter, has been thoroughly investigated in our laboratory.<sup>15, 16</sup> All evidence suggests that the cellular uptake of octahedral metal complexes occurs via passive diffusion, with an increase in the hydrophobicity of the ancillary ligands of a complex dramatically enhancing uptake. These trends, however, were elucidated using the  $\text{Ru(L)}_2(\text{dppz})^{2+}$  family of complexes, not larger, more complex, bifunctional conjugates. While studies are currently underway involving Ru-peptide conjugates, much remains to be done to fully understand the uptake of these more complex systems.

The second factor, reduced DNA binding affinity, is more central to the investigations at hand. It has been empirically observed that the binding affinity of the



**7.2: Some mismatch-specific bifunctional conjugates.** Four bifunctional conjugates previously developed by this laboratory. Metalloinsertors were employed to impart mismatch-specificity on pendant alkylating<sup>12</sup> (A), platinating<sup>13</sup> (B), fluorescent<sup>14</sup> (C), and DNA cleaving<sup>11</sup> (D) agents.

mismatch-specific conjugates (and their rhodium subunits alone) are lower than that of their parent  $\text{Rh}(\text{bpy})_2(\text{chrysi})^{3+}$ ,  $\text{Rh}(\text{bpy})(\text{phen})(\text{chrysi})^{3+}$ , and  $\text{Rh}(\text{phen})_2(\text{chrysi})^{3+}$  complexes.<sup>11, 13, 14</sup> All of the bifunctional conjugates to date have employed a  $\text{Rh}(\text{phen})(\text{chrysi})(^x\text{bpy})^{3+}$  framework as their metalloinsertor subunit, where  $^x\text{bpy}$  denotes a 4,4'-dimethyl-bipyridine ligand with one of the methyl groups alkylated to create a linker moiety. These metalloinsertors exist as a mixture of four stereoisomers, two enantiomers of two diastereomers (**Figure 7.3**).<sup>a</sup> The enantiomers, of course, are born out of the innate chirality of octahedral metal complexes containing three bidentate ligands. The diastereomers, in contrast, are created by the asymmetry of the linker-modified bipyridine ligand; the linker-modified methyl can either be perpendicular (axial diastereomer) or parallel (equatorial diastereomer) to the plane of the chrysi ligand.

It is known from past experiments that neither  $\Lambda$ -enantiomer will effectively bind mismatched DNA.<sup>17-19</sup> This, however, is true of all known metalloinsertors, and thus will not reduce the binding affinity of the conjugates relative to other mismatch-specific complexes. The problem, then, lies in the linker-modified bipyridine ligand, predominantly the linker itself but also the complementary methyl group. The relationship between ancillary ligand bulk and DNA binding affinity has been firmly established: the larger the ancillary ligands, the weaker the complex binds DNA. The recent work of Ernst and Song in our laboratory has illustrated this quite nicely. As the ancillary ligands get larger — from  $\text{Rh}(\text{NH}_3)_4(\text{chrysi})^{3+}$  to  $\text{Rh}(\text{bpy})_2(\text{chrysi})^{3+}$  to  $\text{Rh}(\text{DIP})_2(\text{chrysi})^{3+}$  — the binding affinity of a complex for a C•C mismatch drops dramatically, from  $1 \times 10^8 \text{ M}^{-1}$  to  $3.4 \times 10^7 \text{ M}^{-1}$  to  $9.1 \times 10^4 \text{ M}^{-1}$ , respectively.<sup>9</sup> It follows

---

<sup>a</sup> As they are almost certainly inconsequential from a DNA-binding stand-point, the diastereomers resulting from the asymmetry of the chrysi ligand are typically ignored.

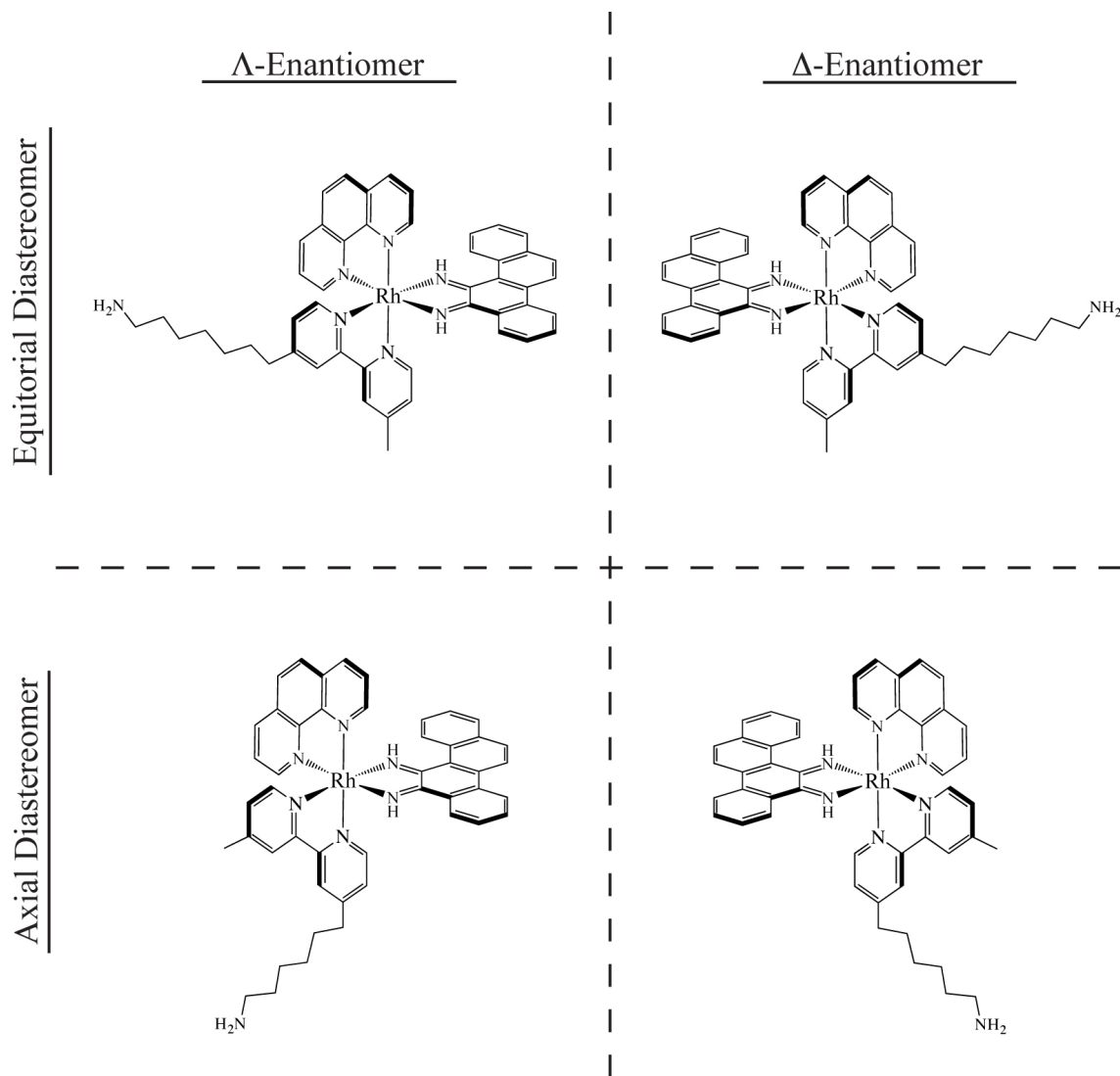


**Figure 7.3:** The stereoisomers of  $\text{Rh}(\text{phen})(\text{chrysi})(\text{NH}_2\text{bpy})^{3+}$ . It is almost certain that neither  $\Delta$ -enantiomer binds mismatched DNA, but it is likely that the affinities of both  $\Delta$ -enantiomers are reduced relative to the parent complexes as well.

that the  $\Delta$ -enantiomers of  $\text{Rh}(\text{phen})(\text{chrysi})(^x\text{bpy})^{3+}$  may also have reduced binding affinity relative to their parent complexes. The affinity of the axial diastereomer is likely particularly reduced due to the large linker that likely clashes significantly with the phosphate backbone above or below the binding site of the complex. The equatorial diastereomer may be similarly affected by the bulk of its axially-positioned methyl group, though perhaps to a lesser degree.

Mismatch-specific bifunctional conjugates have tremendous potential, and thus we could not just throw in the towel. Therefore, to remedy this binding affinity problem, we have recently turned to a new platform for linker-modified ligands: 2,2'-dipyridylamine (HDPA, **Figure 7.4**). The key to HDPA is the centrally located, bridging nitrogen. This central amine can be alkylated to yield a linker-modified dipyriddyamine (DPA) ligand (see CHAPTER 2 for synthetic protocols). Upon metallation, the linker thus extends diagonally from the metal complex, reducing the steric clash that hindered the binding of the metalloinsertors bearing modified dimethyl-bipyridine ligands. Further, the two-fold symmetry of the modified DPA ligands eliminates any diastereomers in trisheteroleptic complexes;  $\text{Rh}(\text{phen})(\text{chrysi})(\text{DPA}')^{3+}$ , for example, exists simply as a mixture of  $\Delta$ - and  $\Lambda$ -enantiomers.

Experiments with  $\text{Rh}(\text{bpy})_2(\text{chrysi})^{3+}$  and  $\text{Rh}(\text{HDPA})_2(\text{chrysi})^{3+}$  have shown that switching from bipyridine to dipyriddyamine ancillary ligands does not result in any substantive reduction in site-specific affinity. More important still, the C•C mismatch-specific binding constant of  $\text{Rh}(\text{phen})(\text{chrysi})(\text{HDPA})^{3+}$  is  $2.5 \times 10^6 \text{ M}^{-1}$ , and only a slight reduction in affinity is observed for the analogous complex bearing a DPA ligand with a carboxylate-terminated linker ( $9.8 \times 10^5 \text{ M}^{-1}$ ).

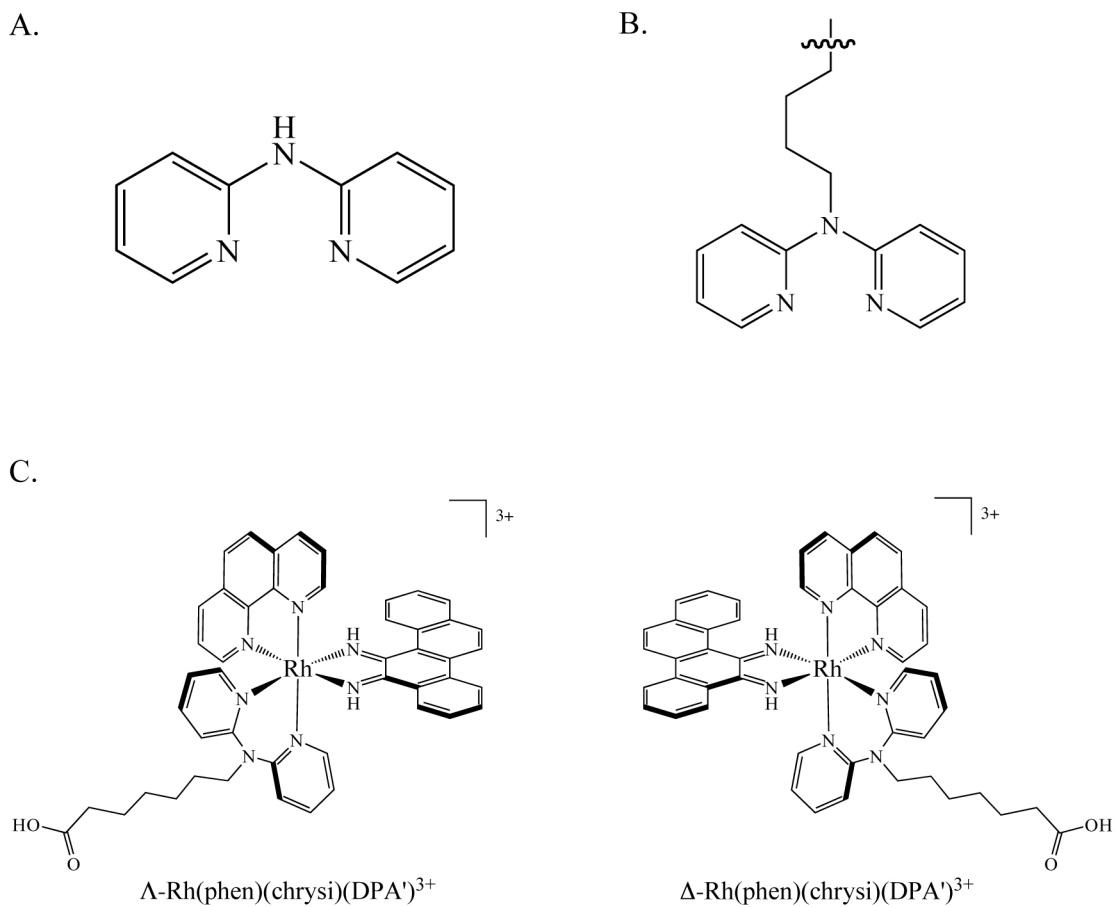


**Figure 7.4: A new option for linker-modified ligands.** (A) 2,2'-dipyridylamine (HDPA); (B) a linker-modified dipyriddyamine (DPA) ligand; (C) the  $\Lambda$ - and  $\Delta$ -enantiomers of Rh(phen)(chrysi)(DPA')<sup>3+</sup> (left and right, respectively).

There is, however, one significant limitation to HDPA and modified DPAs as ligands for metalloinsertors: altered photochemistry.  $\text{Rh}(\text{HDPA})_2(\text{chrysi})^{3+}$ , for example, is not photochemically active and, therefore, is unable to affect photocleavage at its binding site.<sup>b</sup> Complexes bearing at least one bipyridine-based ligand fare slightly better;  $\text{Rh}(\text{phen})(\text{chrysi})(\text{HDPA})^{3+}$  is capable of site-specific, photoactivated strand scission, but at drastically reduced efficiencies compared to  $\text{Rh}(\text{bpy})_2(\text{chrysi})^{3+}$  or  $\text{Rh}(\text{phen})(\text{chrysi})(\text{bpy})^{3+}$  (**Figure 7.5**). Fortunately, while photocleavage is useful for the characterization of metalloinsertors and their conjugates, it becomes less important in the *in vivo* applications for which most bifunctional conjugates are intended.<sup>c</sup>

No bifunctional conjugates employing a modified dipyriddyamine ligand have yet been published, though a number are currently in development. Herein, we will present two case studies in the design, synthesis, and application of mismatch-specific, bifunctional conjugates. The first, a conjugate bearing a hydrolysable platinum agent, was developed in the era of linker-modified bipyridine ligands. The second, a metalloinsertor-radionuclide conjugate, employs a linker-modified dipyriddyamine ligand. Both cases offer significant insights into the factors important for the successful development of useful, mismatch-specific bifunctional conjugates and will hopefully inspire continued research into these molecules and others like them.

---

<sup>b</sup> The binding constant for this compound was determined via competition with  $\text{Rh}(\text{bpy})_2(\text{chrysi})^{3+}$  (see chapter 2 for details).

<sup>c</sup> As an aside, a third option exists that may combine the best features of bipyridine (photochemistry) and dipyriddyamine (linker location) ligands: linker-modified 3-methyl-2,2'-bipyridine ligands. 3-methyl-2,2'-bipyridine can be synthesized via the facile cross-coupling of 2-pyridylzinc bromide and 2-chloro-3-methyl pyridine. The bipyridine product can then be alkylated and converted to ligand with a useful linker via the protocols described in Chapter 2. See Notebook 6, Page 116 for a cross-coupling procedure.

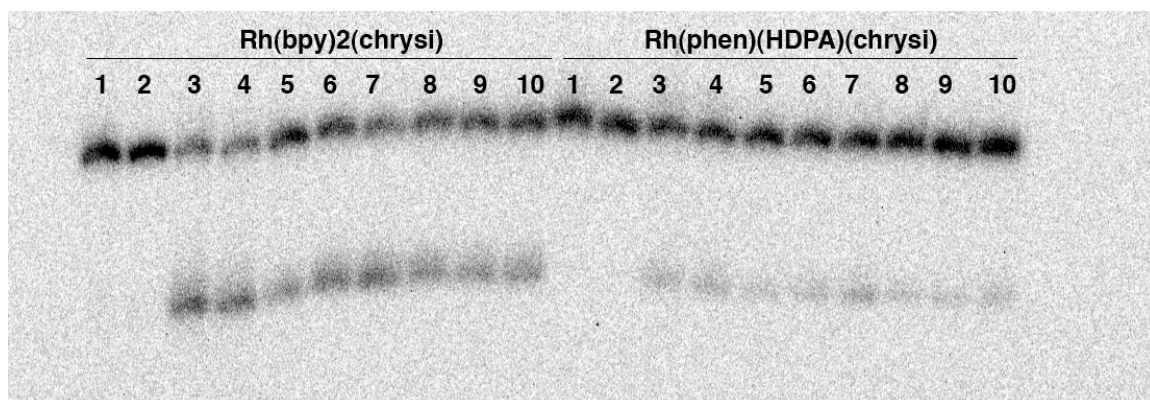


**Figure 7.5: The reduced photocleavage efficiency of  $\text{Rh(phen)(HDPA)(chrysi)}^{3+}$ .**

Autoradiogram of a denaturing 20% polyacrylamide gel showing the mismatch-specific DNA photocleavage of  $\text{Rh(bpy)}_2(\text{chrysi})^{3+}$  and  $\text{Rh(phen)(HDPA)(chrysi)}^{3+}$  as a function of irradiation wavelength. Conditions are duplex (5  $\mu\text{M}$ ), Rh (5  $\mu\text{M}$ ) in 20 mM NaCl, 10 mM NaPi, in pH 7.1 followed by irradiation for 12 min. The left set of lanes contains  $\text{Rh(bpy)}_2(\text{chrysi})^{3+}$ , while the right set of lanes contains  $\text{Rh(phen)(HDPA)(chrysi)}^{3+}$ .

Lane 1: matched DNA, irradiation with solar simulator. Lane 2: mismatched DNA, dark control. Lanes 3–10 contain mismatched DNA irradiated at wavelengths of 300, 320, 340, 360, 380, 400, 420, and 440 nm, respectively. The DNA sequence is 5'- $^{32}\text{P}$ -GCA TCG ACA GAC CAG CTT ATC AT**C** CTA AGA GCG – 3' where the bold, red C is complementary to a G in the matched duplex and a C in the mismatched duplex. Note the reduced photocleavage efficiency of  $\text{Rh(phen)(HDPA)(chrysi)}^{3+}$  at all wavelengths.

Independent experiments indicate the binding affinities of the two complexes are similar.

## 7.2: A SECOND GENERATION METALLOINSERTOR-PLATINUM CONJUGATE

### 7.2.1: INTRODUCTION

Cisplatin, *cis*-Pt(NH<sub>3</sub>)<sub>2</sub>Cl<sub>2</sub>, is the original member of a family of extensively employed and highly effective platinum-based chemotherapeutic agents that have been used to combat a wide variety of cancers, including carcinomas, sarcomas, and lymphomas (**Figure 7.6**).<sup>20, 21</sup> *In vivo*, cisplatin exerts its biological effect by making covalent, intrastrand DNA crosslinks to purine bases, most often guanine doublets; these DNA adducts activate the cellular DNA damage response, interfere with cell division, and ultimately trigger cell death.<sup>22-30</sup> Some cancers, including many linked with mismatch repair deficiency, have proven resistant to cisplatin.<sup>31-37</sup> This phenomenon and the harsh side effects associated with cisplatin chemotherapy have fueled considerable research into the development of new, more effective, and less toxic platinum(II) chemotherapeutics.<sup>38</sup> Two of the most successful, carboplatin and oxaliplatin, are currently widely employed in chemotherapeutic protocols. Carboplatin, like cisplatin, bears two *cis*-ammine ligands.<sup>39</sup> Oxaliplatin, in contrast, employs a 1*R*,2*R*-(-)-*trans*-diaminocyclohexyl (dach) ligand that has been shown to restore drug activity in many cisplatin resistant cell lines.<sup>40</sup> Interestingly, in order to improve the ligand exchange kinetics of the Pt(II) center, both drugs employ hydrolysable dicarboxylate ligands in place of the chlorides of cisplatin.

Given the cisplatin resistance of many cancers linked to mismatch-repair deficiency, we have hypothesized that the conjugation of a platinum(II) chemotherapeutic subunit to a mismatch-specific metalloinsertor may successfully modulate the toxicity of

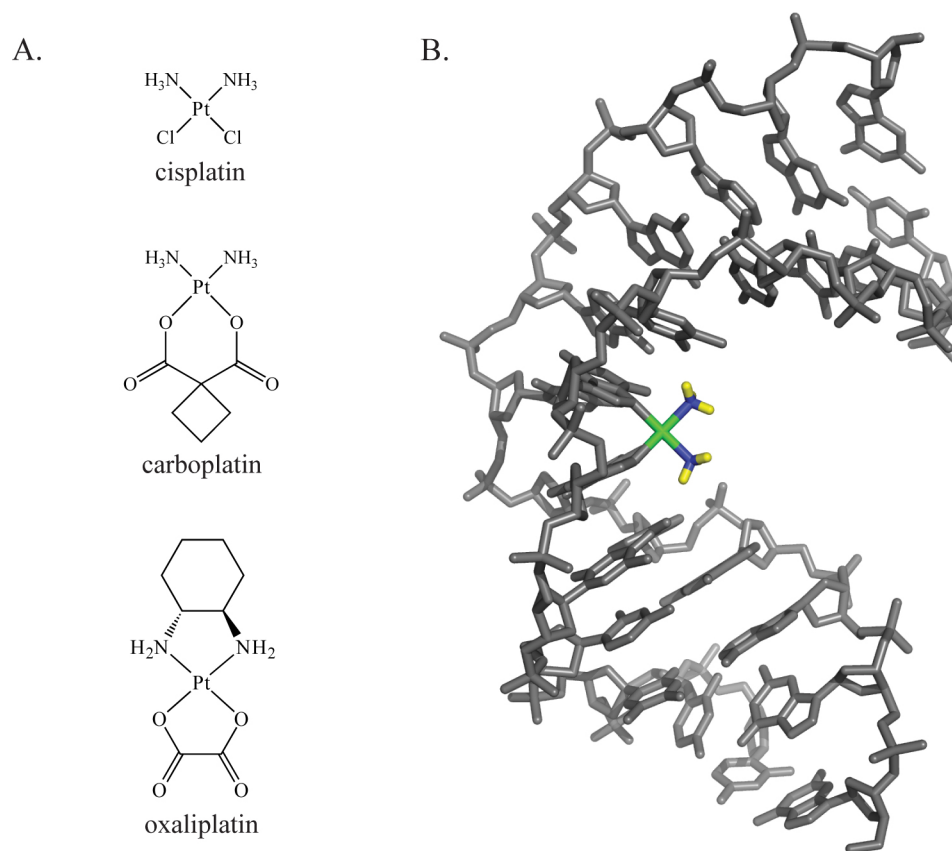


**Figure 7.6: Platinum(II)-based chemotherapeutics.** (A) Three commonly-employed platinum(II) drugs. (B) An NMR structure revealing the kink induced in DNA upon the formation of a 1,2-intrastrand d(GpG) adduct by cisplatin.<sup>41</sup>

the drug to these types of tumors. In essence, the metalloinsertor would act as a molecular taxi, selectively delivering the platinum agent to mismatched DNA and thus concentrating the drug in those cells replete with mismatches (i.e. MMR-deficient cells). We have previously designed, synthesized, and tested a first generation metalloinsertor-platinum conjugate (RhPt1, **Figure 7.2B**).<sup>13</sup> The conjugate successfully and selectively delivers its platinum cargo to mismatched DNA; however, it is limited by the permanent covalent link between the metalloinsertor and platinum subunits. Because the linker connects the metalloinsertor to the non-labile 1,2-diaminoethane ligand of the platinum moiety, the platinum complex can only form adducts with DNA within a linker-length of the binding site of the metalloinsertor.

We have set out to design and synthesize a second generation metalloinsertor-platinum conjugate, RhPt2, to address these limitations. In this case, the platinum subunit is inspired by oxaliplatin, containing both a diaminocyclohexyl ligand known to combat cisplatin resistance and a dicarboxylate, malonate-derived ligand.<sup>38, 42</sup> The metalloinsertor subunit is linked to the platinum moiety not through the inert diammine ligand but rather through the hydrolysable malonate-derivative ligand. Kinetic studies on oxaliplatin and related platinum complexes have shown that the hydrolysis half-lives of their dicarboxylate ligands is around 3 h at 37 °C.<sup>39</sup> Thus, this conjugate, like RhPt1, will act as a molecular taxi, but this time, however, it will drop its passenger off. The intact conjugate will first seek out and selectively bind mismatched DNA; then, on a longer timescale, the platinum unit will be released from the conjugate by hydrolysis and will be free to form its cytotoxic adducts with any of the DNA in the nucleus of the targeted cell.

### 7.2.2: SYNTHESIS

The conjugate was synthesized in a convergent manner, with the rhodium and platinum moieties completed separately and coupled in the final step. The trisheteroleptic, linker-modified rhodium subunit,  $\text{Rh}(\text{phen})(\text{chrysi})(\text{NH}_2\text{bpy})^{3+}$ , was synthesized from  $\text{RhCl}_3$  according to standard protocols (**Figure 7.7**, see Chapter 2).<sup>2, 12</sup>

The platinum subunit presented a more original, if not slightly more difficult, synthetic challenge.<sup>d,43</sup> First, the dicarboxylate ligand was synthesized. To provide further space between the platinum and rhodium moieties and to enable efficient coupling, a 2-(4-carboxybenzylidene)malonic acid ligand was employed and synthesized via either of two routes from paraformylbenzoic acid (**Figure 7.8**). In method 1, the benzoic acid is protected with a tert-butyl ester, reacted with dibenzyl malonate via a  $\text{TiCl}_4$ -promoted Knoevenagel condensation, and selectively deprotected with hydrogen over Pd/C to yield t-butyl-protected 2-(4-carboxybenzylidene)malonic acid (MalBzCOOtBu). In the second, more efficient route, the Knoevenagel condensation comes first.

Paraformylbenzoic acid is reacted with dibenzyl malonate in the presence of  $\text{TiCl}_4$ , and the free carboxylic acid of this product is protected with a tert-butyl ester via acid-catalyzed reaction with isobutene. A subsequent, selective deprotection step with  $\text{H}_2$  over Pd/C yields the completed MalBzCOOtBu.

The completed malonate ligand was metallated via reaction with  $\text{Pt}(\text{dach})(\text{NO}_2)_2$ , a platinum(II) species prepared in two steps from  $\text{K}_2\text{PtCl}_4$  (**Figure 7.9**). Finally, the ready-to-couple Pt2 subunit,  $\text{Pt}(\text{dach})(\text{MalBzCOOH})$ , was obtained via deprotection of

---

<sup>d</sup> For much of the synthetic work on the platinum subunit of RhPt2, I am deeply indebted to the prodigious talents of Dr. Anne Petitjean, a former postdoctoral researcher in the Barton laboratory.

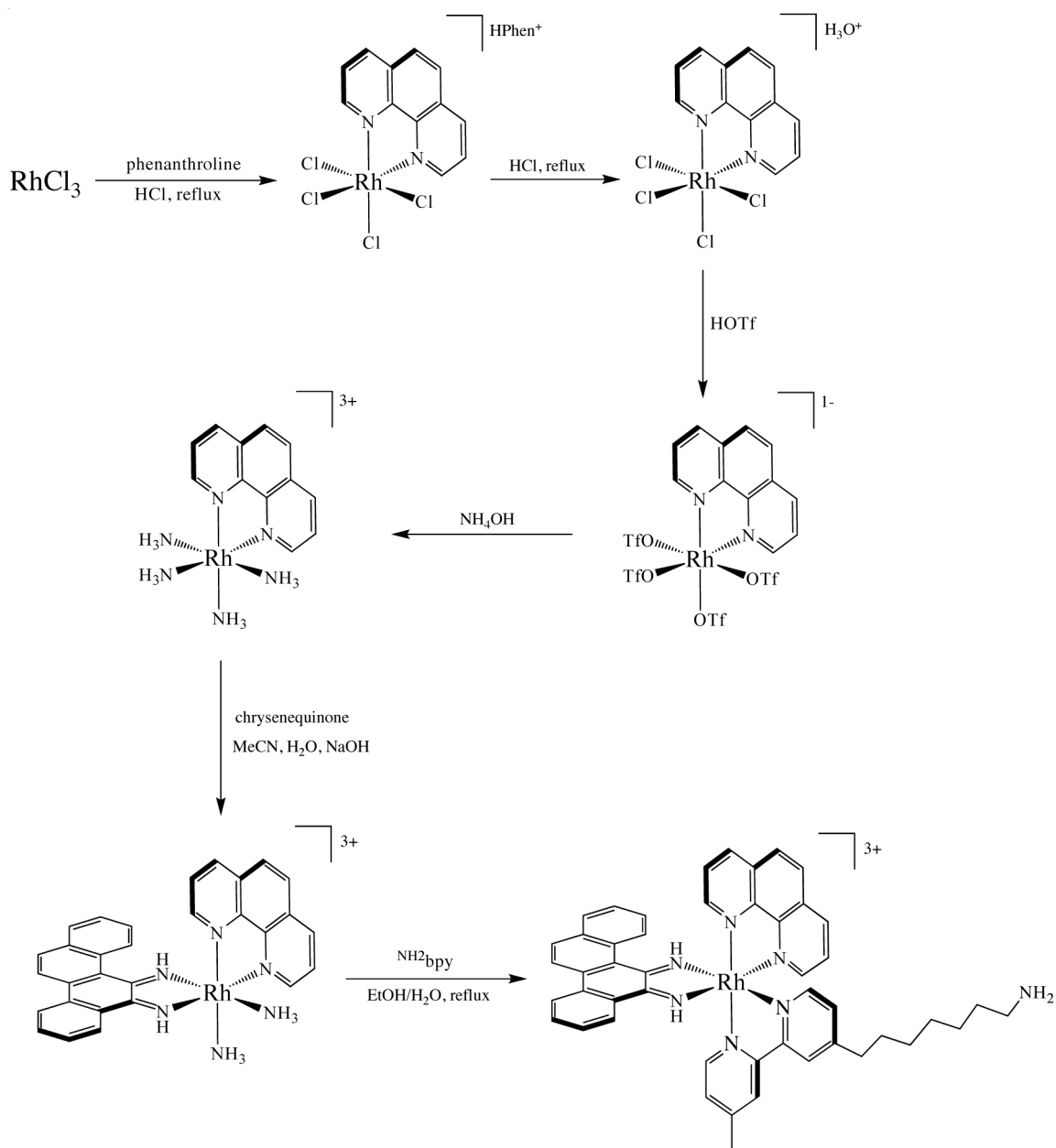


**Figure 7.7. The synthetic route to the trisheteroleptic metalloinsertor subunit.** The conjugate's metalloinsertor subunit was synthesized via the sequential addition of phen, chrysi, and  $\text{NH}_2\text{bpy}$  ligands onto a rhodium center.

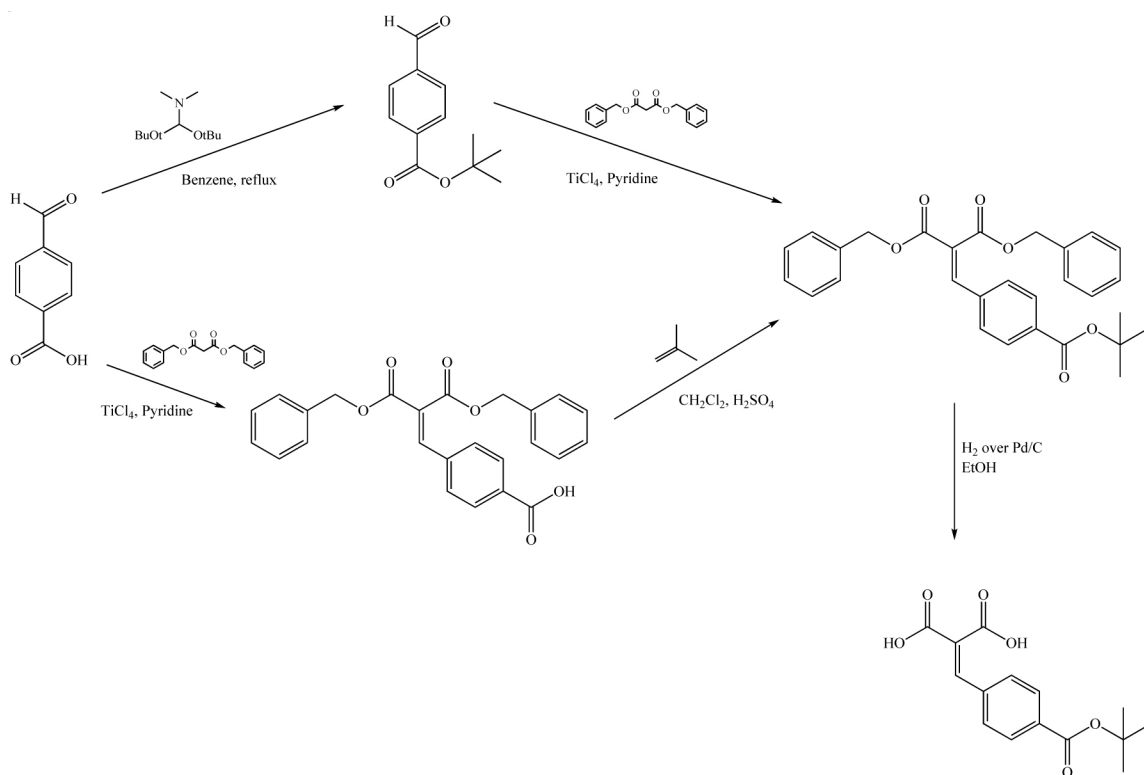


**Figure 7.8: The synthetic route to the Pt<sub>2</sub> malonate ligand.** The ligand can be synthesized from paraformylbenzoic acid via two routes. In method 1 (top), the carboxylic acid is first protected, followed by a Knoevenagel condensation with dibenzyl malonate. In method 2 (bottom), the Knoevenagel condensation with dibenzyl malonate comes first and is followed by the protection of the free carboxylic acid. Regardless of which method is followed, the benzyl esters of the resultant product are then removed with  $\text{H}_2$  over  $\text{Pd/C}$ , yielding the protected Pt<sub>2</sub> malonate ligand that is ready for metallation onto Pt(II).

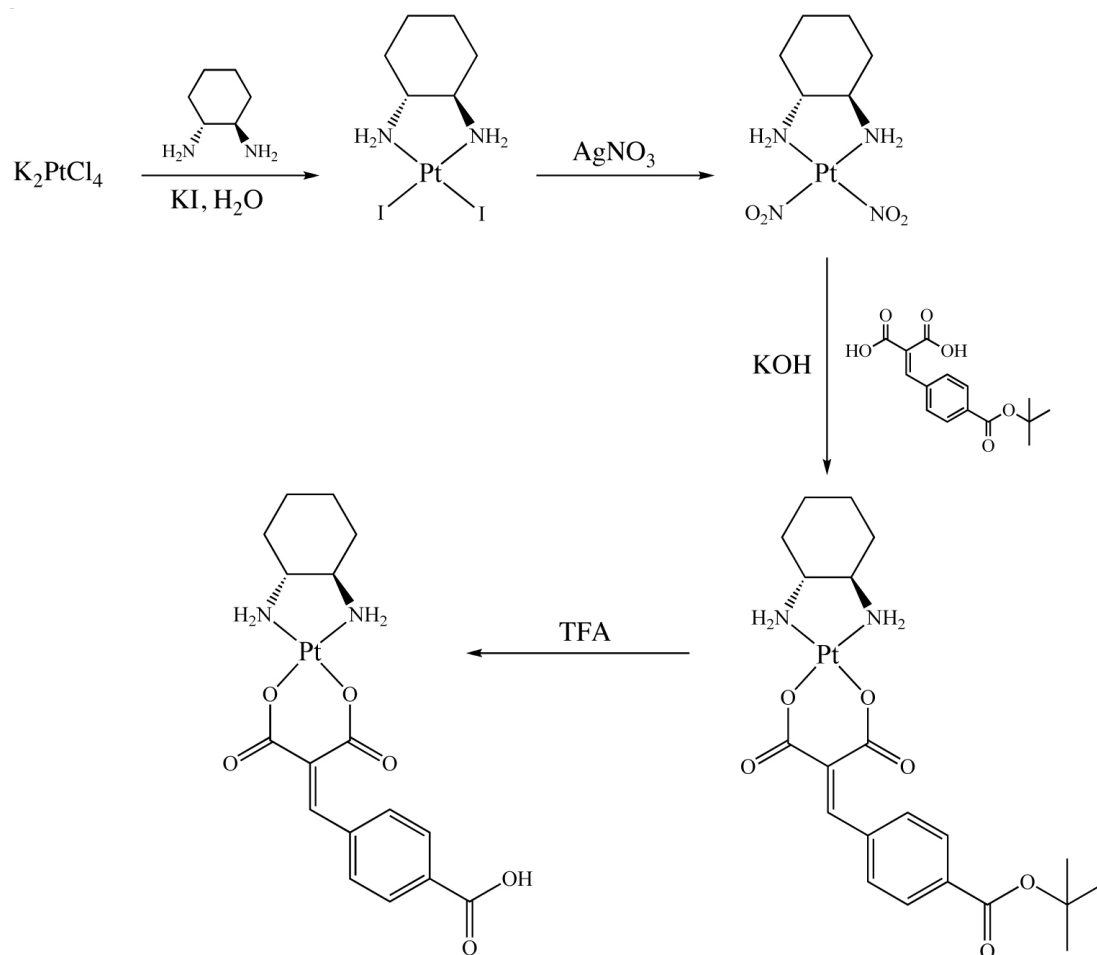


**Figure 7.9: The synthetic route to Pt2.**  $Pt(dach)(NO_2)_2$  is prepared in two steps from potassium tetrachloroplatinate via ligand substitution reactions. The t-butyl ester-protected malonate ligand is then metallated onto the platinum center in the presence of base to produce  $Pt(dach)(MalBzCOOtBu)$ , and this complex is deprotected with TFA to yield the ready-to-couple Pt2 product.

the tert-butyl ester with trifluoroacetic acid. The completed RhPt2 conjugate was then obtained via peptide coupling with Rh(phen)(chrysi)(<sup>NH2</sup>bpy)<sup>3+</sup> using HATU (**Figure 7.10**) and purified via cation exchange (Sephadex CM-25) and reverse-phase HPLC chromatography.

### 7.2.3: MISMATCH RECOGNITION AND PLATINATION EXPERIMENTS

The mismatch recognition and DNA platination properties of RhPt2 were investigated with denaturing polyacrylamide gel electrophoresis using radiolabeled oligonucleotides that contain both a d(GpG) target site (blue) for platination and a central C•C mismatch (red) for metalloinsertor binding: 5'-<sup>32</sup>P-TTA GGA TCA TCC ATA TA-3'. Control experiments with matched (C•G) duplexes were also performed, but controls using DNA without a d(GpG) binding site were deemed unnecessary, because the platinum(II) complex will readily bind other purine sites in the absence of its preferred guanine doublet target. Experiments previously performed with the original RhPt1 conjugate tell us what to look for; while mismatch-site strand scission products naturally travel more quickly on a gel than their parent DNA strands, platination products travel more slowly and thus appear above the parent band in the gel.

A simple recognition and photocleavage assay clearly illustrates that the RhPt2 conjugate specifically recognizes and photocleaves mismatched DNA (**Figure 7.11**). In these recognition experiments, RhPt2 was incubated with the DNA for very short amounts of time before irradiation in order to minimize the number of platinum adducts formed. Subsequently, binding constant titrations revealed that the site-specific affinity of

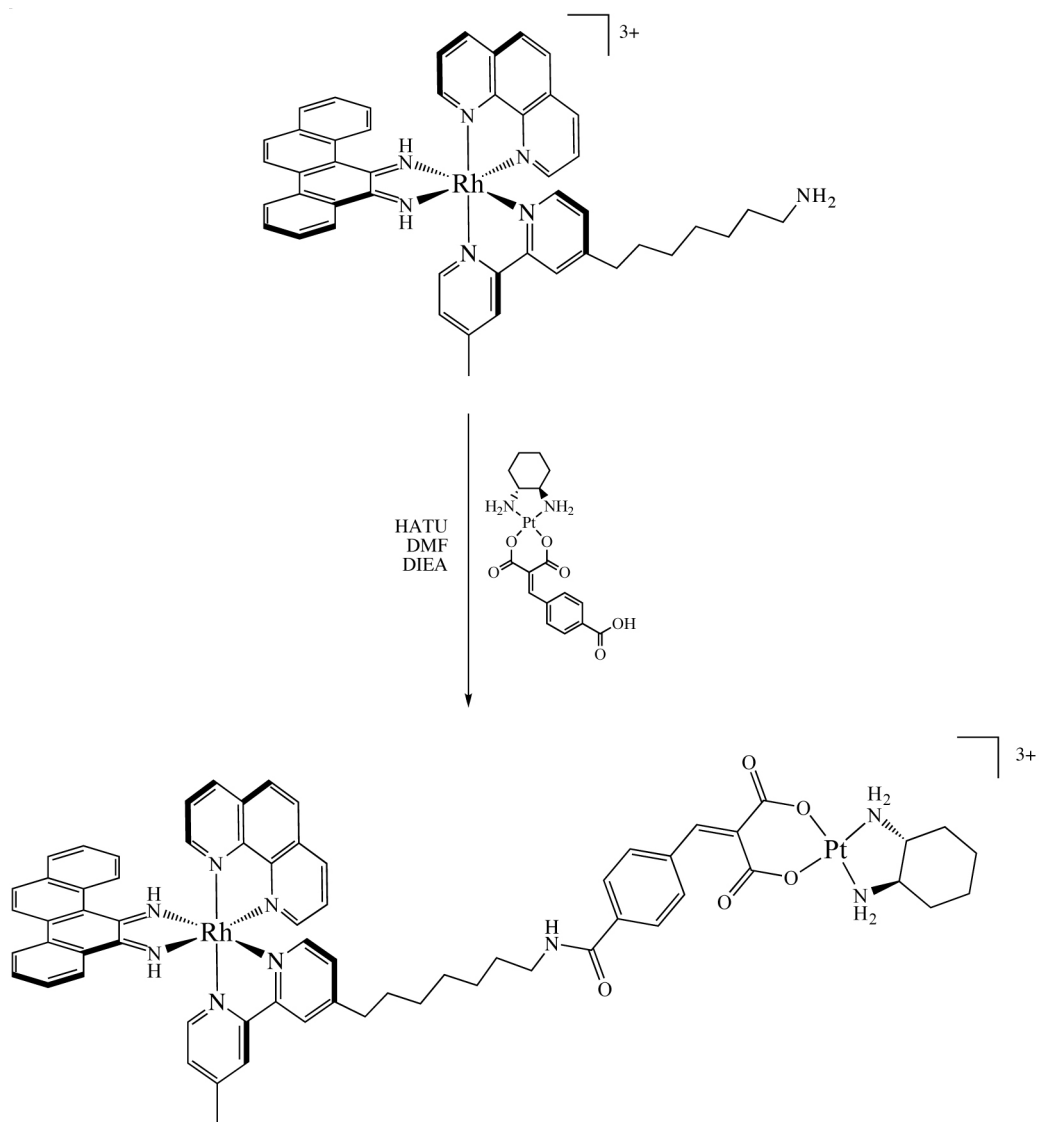


**Figure 7.10: The synthesis of RhPt2.** To form RhPt2, Pt2 [Pt(dach)(MalBzCOOH)] and Rh(phen)(chrysi)(<sup>NH2</sup>bpy)<sup>3+</sup> are coupled with HATU.

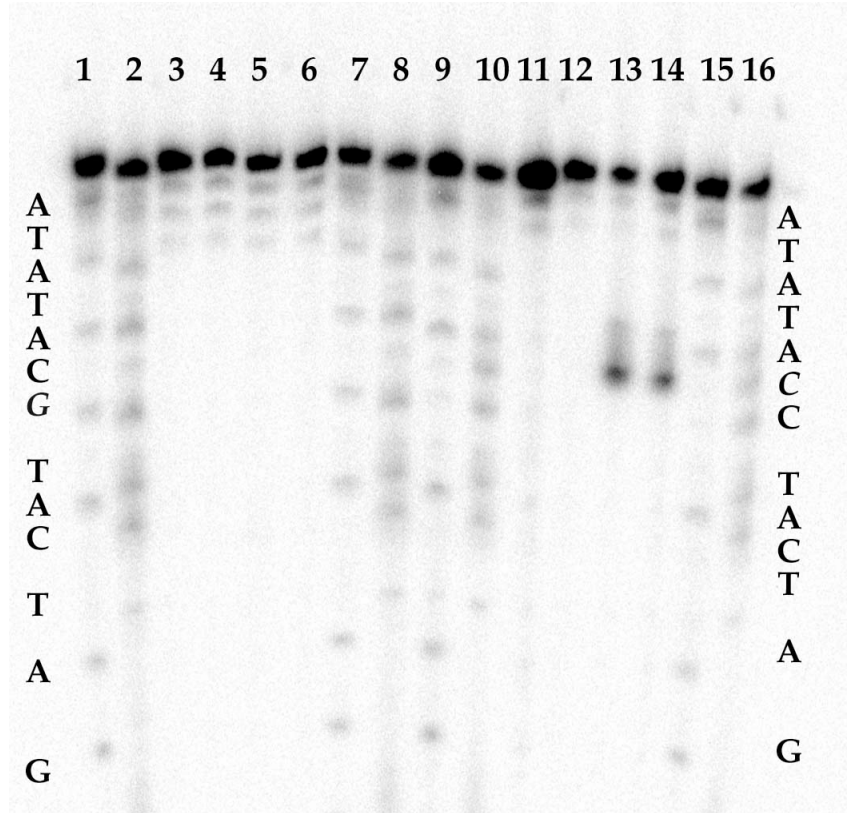


**Figure 7.11: Mismatch recognition and photocleavage of RhPt2.** Autoradiogram of a denaturing 20% polyacrylamide gel showing the mismatch-specific DNA photocleavage of RhPt2. Conditions are duplex (2  $\mu$ M) and RhPt2 (2  $\mu$ M) in 20 mM NaCl, 10 mM NaPi, pH 7.1 followed by irradiation on an Oriel Instruments solar simulator (320–440 nm). Lanes 1, 2, 7, and 8 are Maxam Gilbert A+T (1, 7) and C+G (2, 8) sequencing reactions for matched DNA. Lane 3 contains a matched DNA light control. Lane 4 contains a matched DNA dark control. Lanes 5 and 6 contain matched DNA and metal complex with irradiation for 3 and 6 min, respectively. Lanes 9, 10, 15, and 16 are Maxam Gilbert A+T (1, 7) and C+G (2, 8) sequencing reactions for mismatched DNA. Lane 11 contains a mismatched DNA light control. Lane 12 contains a mismatched DNA dark control. Lanes 13 and 14 contain mismatched DNA and metal complex with irradiation for 3 and 6 min, respectively. The DNA sequence is 5'-<sup>32</sup>P-TTA GGA TCA **TCC** ATA TA-3' where the bold, red C is complementary to a G in the matched duplex and a C in the mismatched duplex.

RhPt2 for a C•C mismatch is approximately  $1 \times 10^6 \text{ M}^{-1}$ , though the plot of RhPt2 concentration against photocleavage produces a somewhat skewed sigmoid, so the actual value is likely lower.

Additional electrophoresis experiments allowed for the interrogation of the platination behavior of RhPt2. Simple incubation experiments with radiolabeled matched and mismatched duplexes reveal that clear, slow-moving platination adducts are formed when DNA is incubated with RhPt2 for 3 hours (**Figure 7.12**). A comparison to the products formed upon incubation of DNA with cisplatin suggests that the adducts formed by RhPt2 move more slowly through the gel and thus are slightly different; this is not surprising given the greater steric bulk of the diaminocyclohexyl ligand of the Pt2 complex. Further, more careful examination of the cisplatin-containing lanes reveals that a second, even more slowly moving adduct is formed during these incubations. Notably, the same is true with RhPt1, and in that case, it was hypothesized that the two bands represent intra- and interstrand platination adducts.<sup>13</sup> The greater steric bulk of the diaminocyclohexyl ligand of Pt2 may also be responsible for the absence of a second, likely interstrand platination product in the case of RhPt2.

Perhaps not surprisingly given the hydrolysis of the Pt2 subunit, platination adducts are observed with both matched and mismatched duplexes. Further still, experiments to probe the platination selectivity of RhPt2 in the presence of mixtures of matched and mismatched assemblies reveal that the Pt2 unit shows little specificity for the platination of mismatched DNA. It seems that even though the metalloinsertor subunit of the conjugate selectively binds mismatched DNA, the platinum subunit, once released, is free to bind either matched or mismatched DNA with little discrimination.

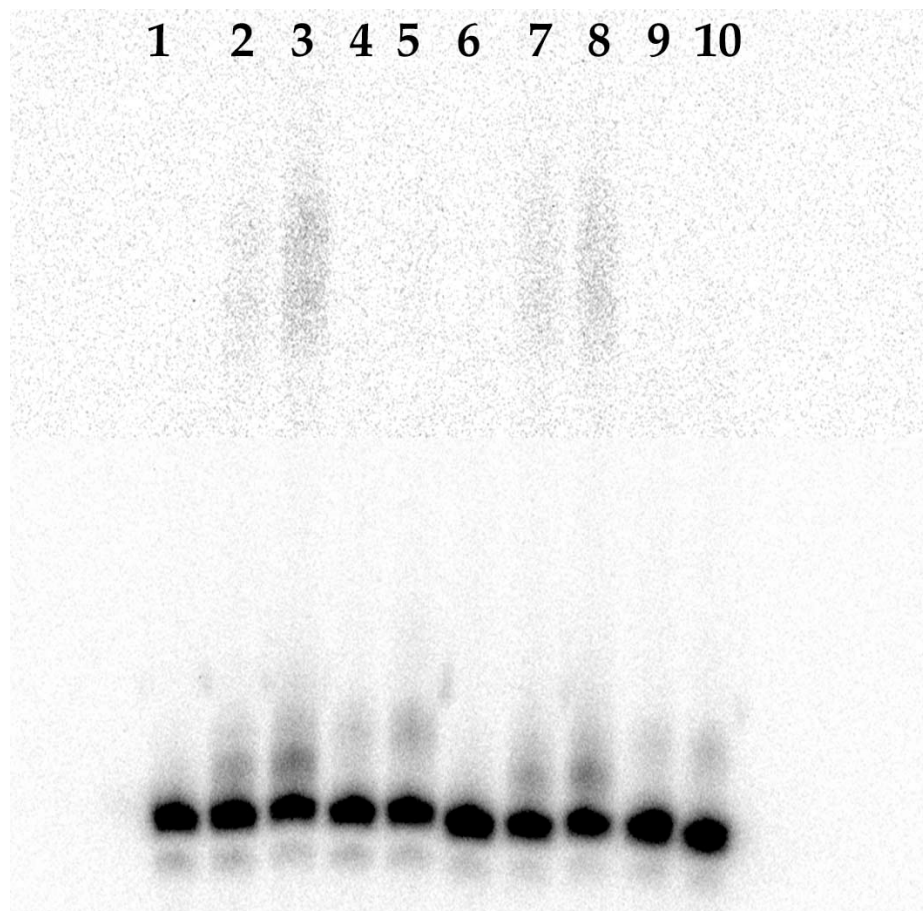


**Figure 7.12: DNA platination adducts formed by cisplatin and RhPt2.** Autoradiogram of a denaturing 20% polyacrylamide gel showing the platination adducts formed by cisplatin and RhPt2. Conditions are duplex (2  $\mu\text{M}$ ) in 20 mM NaCl, 10 mM NaPi, pH 7.1 with three hour incubations. Lanes 1–5 contain matched DNA. Lanes 6–10 contain mismatched DNA. Lanes 1 and 6: control, no metal complex. Lanes 2 and 7: DNA with 1  $\mu\text{M}$  cisplatin. Lanes 3 and 8: DNA with 2  $\mu\text{M}$  cisplatin. Lanes 4 and 9: DNA with 1  $\mu\text{M}$  RhPt2. Lanes 5 and 10: DNA with 2  $\mu\text{M}$  RhPt2. The DNA sequence is 5'-<sup>32</sup>P-TTA GGA TCA **TCC** ATA TA-3' where the bold, red C is complementary to a G in the matched duplex and a C in the mismatched duplex. The gain on the top half of the gel has been increased in order to visualize the second platination bands in the cisplatin lanes.

An interesting interplay between platination and photocleavage is also observed at long incubation times (**Figure 7.13**). As expected, the amount of platination adduct increases with time as RhPt2 is incubated with DNA for 3, 6, and 9 hours. Interestingly, a concomitant decrease in the amount of photocleavage is observed with increasing time (**Figure 7.14**). This may be the result of the kink introduced into DNA upon platinum binding. It is almost certain that kinking the DNA would disrupt metalloinsertion at the mismatch. Thus it follows that if more platinum is bound, less rhodium is bound, and less photocleavage will be observed.

#### **7.2.4: DIFFERENTIAL ANTI-PROLIFERATION EXPERIMENTS**

The ultimate goal of a metalloinsertor-platinum conjugate is its successful application as a chemotherapeutic agent for mismatch repair deficient tumors. Thus, BrdU cell proliferation assays were performed in order to investigate the differential biological effect of RhPt2 on mismatch repair proficient and mismatch repair deficient cell lines. To be more specific, two variants of the HCT116 colorectal cancer cell line were employed. The two types of cells, HCT116O and HCT116N, are completely isogenic except for the presence or absence of the gene for the essential mismatch repair protein MLH1. HCT116N cells have an intact copy of the gene and are proficient at mismatch repair, while HCT116O cells do not have the gene and are thus mismatch repair deficient.<sup>44</sup> As discussed earlier in this work,  $\text{Rh}(\text{bpy})_2(\text{chrysi})^{3+}$  and  $\text{Rh}(\text{bpy})_2(\text{phzi})^{3+}$  both selectively inhibit the proliferation of HCT116O cells, a biological effect that additional evidence has suggested is related to the mismatch-specific binding of the metalloinsertors.<sup>8,9</sup>

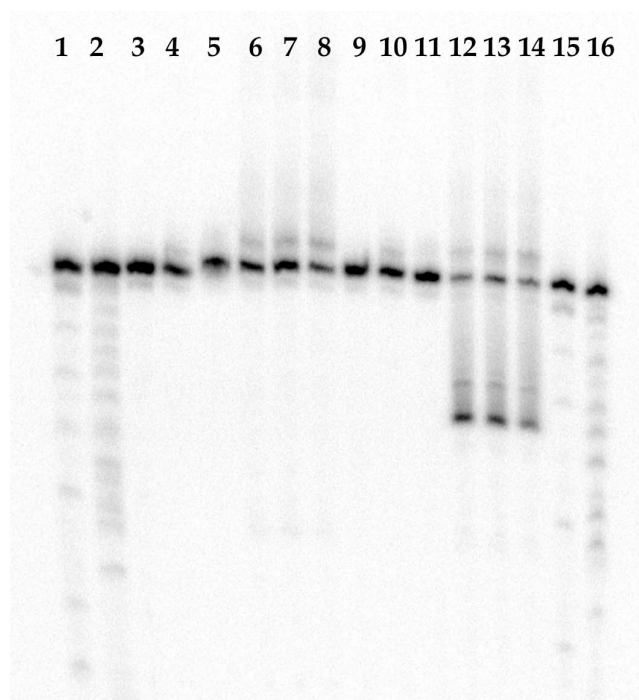


**Figure 7.13: The interplay between photocleavage and platination.** Autoradiogram of a denaturing 20% polyacrylamide gel showing the DNA photocleavage and platination of RhPt2 as a function of incubation time. Conditions are duplex (2  $\mu$ M) and RhPt2 (2  $\mu$ M) in 20 mM NaCl, 10 mM NaPi, pH 7.1 followed by irradiation on an Oriel Instruments solar simulator (320–440 nm). Lanes 1–8 contain matched DNA, and lanes 9–16 contain mismatched DNA. Lanes 1, 2, 15, and 16 are Maxam Gilbert A+T (1, 15) and C+G (2, 16) sequencing reactions. Lanes 3 and 9 contain DNA irradiated for 3 minutes. Lanes 4 and 10 contain DNA with no metal complex and no irradiation. Lanes 5 and 11 contain DNA incubated with RhPt2 for 3 h with no subsequent irradiation. Lanes 5 and 12 contain DNA incubated with RhPt2 for 3 hours with 3 minutes subsequent irradiation. Lanes 6 and 13 contain DNA incubated with RhPt2 for 6 hours with 3 minutes subsequent irradiation. Lanes 7 and 15 contain DNA incubated with RhPt2 for 9 hours with 3 minutes subsequent irradiation. The DNA sequence is 5'-<sup>32</sup>P-TTA GGA TCA **TCC** ATA TA-3' where the bold, red C is complementary to a G in the matched duplex and a C in the mismatched duplex.

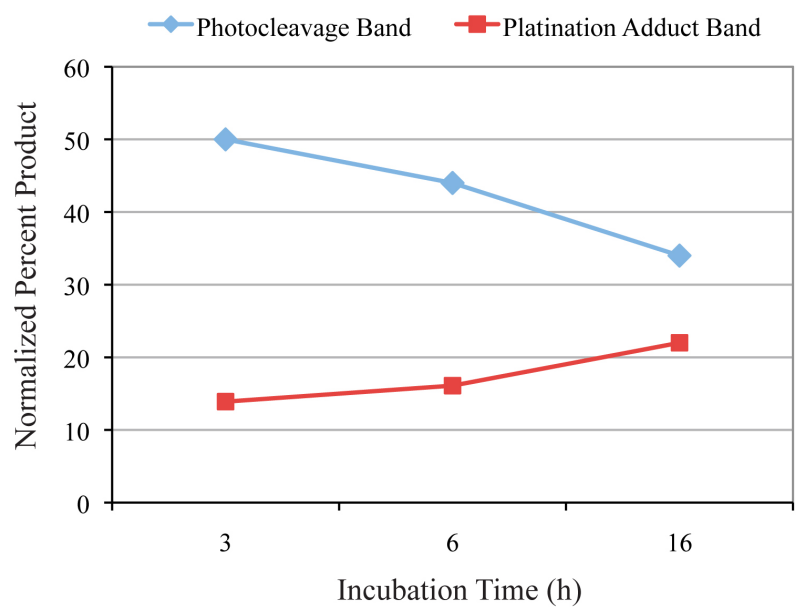


**Figure 7.14: The interplay between photocleavage and platination.** The quantification of lanes 12, 13, and 14 from the gel shown in **Figure 7.13**. Each product is expressed as a percentage of the total DNA in the lane in question.

For the experiments at hand, the adherent HCT116O/N cells were grown in 96-well plates at a concentration of 2000 cells per well. The cells were then incubated with variable concentrations of metal complex for 24 hours, provided fresh media, allowed to grow for 48 hours, and then labeled with BrdU 24 hours before analysis. The amount of BrdU incorporation and, by extension, cellular proliferation was quantified by ELISA assay according to standard procedures.

Consistent with the literature, cisplatin has very little differential antiproliferative effect in the two cell lines; if anything, the complex is slightly more biologically active in the mismatch repair proficient HCT116N cells (**Figure 7.15**).<sup>33–37</sup> The results with RhPt2 are similar (**Figure 7.16**). The conjugate is certainly biologically active, significantly inhibiting cellular proliferation in both cell lines at concentrations as low as 5  $\mu$ M. However, no reliable differential effect is observed. The reasons for this phenomenon are unclear. Two explanations seem most likely. First, the metalloinsertor subunit of the conjugate may have attenuated biological activity compared to its parent  $\text{Rh}(\text{bpy})_2(\text{L})^{3+}$  complexes. Further cell proliferation experiments indicate that this may be at least part of the story, for  $\text{Rh}(\text{phen})(\text{chrysi})(^{\text{NH}_2}\text{bpy})^{3+}$  induces significantly less differential antiproliferative effect in HCT116O/N cells than its parent metalloinsertors. As we have discussed earlier in this chapter, this may be a result of the reduced binding affinity characteristic of trisheteroleptic metalloinsertors with linker-modified 4,4'-dimethylbipyridine ligands. Second, the hydrolysis of the platinum subunit may occur before the metalloinsertor subunit binds the DNA of the cell in question. This, too, seems like it might be part of the story. For as we have learned more about the cellular uptake of octahedral metal complexes, it has become clear that the average uptake time

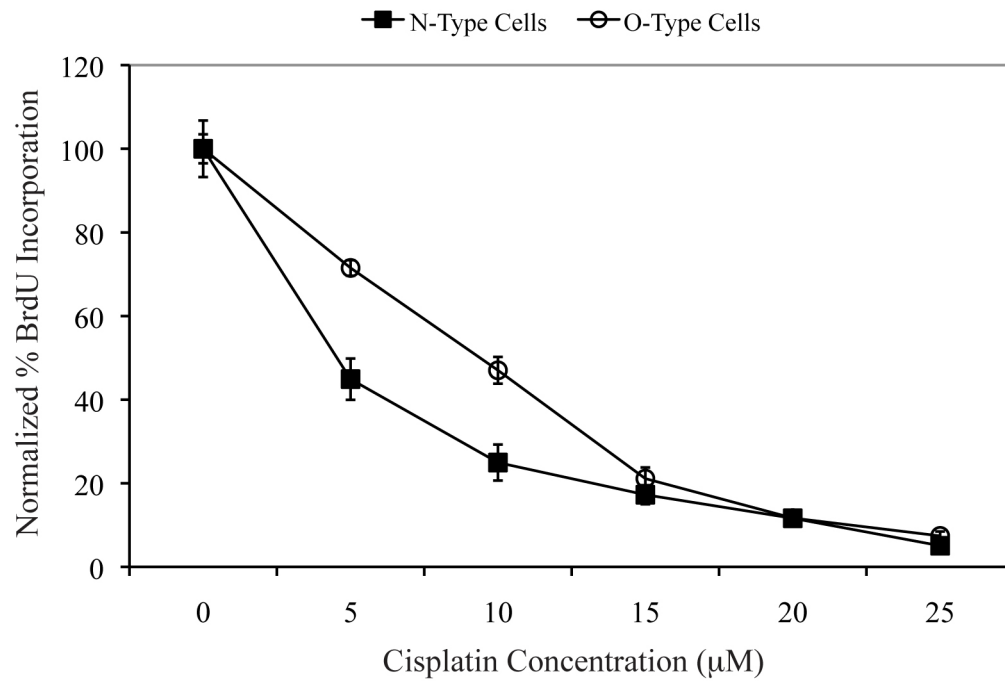


**Figure 7.15: The antiproliferative effects of cisplatin on HCT116O/N cells.** The normalized percent BrdU incorporation (a marker of cell proliferation) in HCT116O (MMR-) and HCT116N (MMR+) cells is shown as a function of cisplatin concentration.

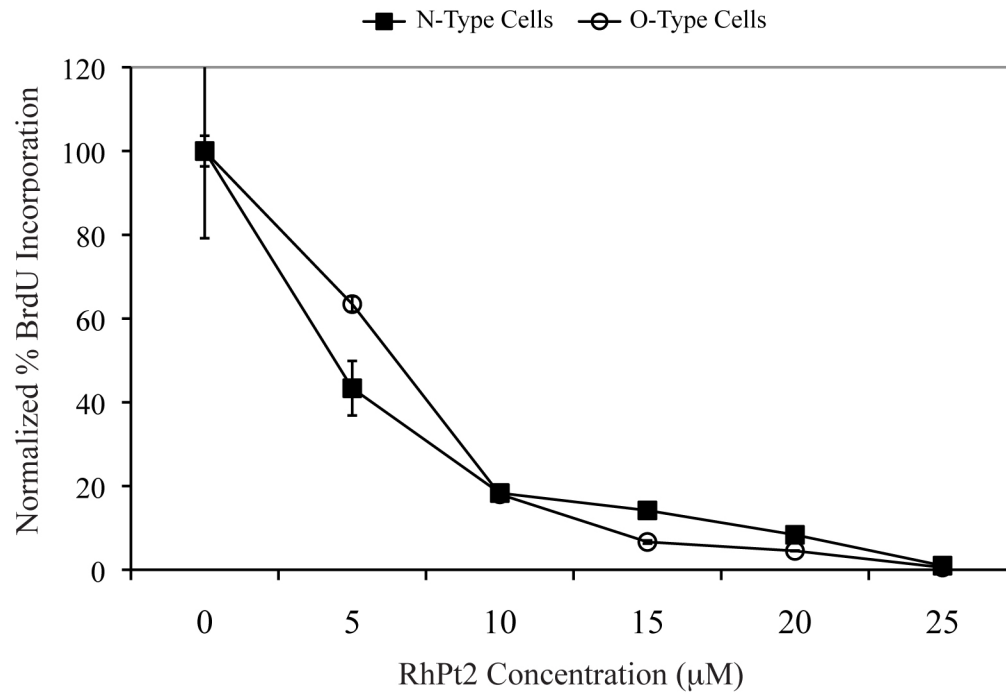


**Figure 7.16: The antiproliferative effects of RhPt2 on HCT116O/N cells.** The normalized percent BrdU incorporation (a marker of cell proliferation) in HCT116O (MMR-) and HCT116N (MMR+) cells is shown as a function of RhPt2 concentration.

for a complex (approximately 12–24 hours) is far longer than the hydrolysis half life of oxaliplatin-like complexes (approximately 3 hours).

### **7.2.5: CONCLUSION**

Gauging the success of a bifunctional conjugate can be difficult. To be sure, the development of the RhPt2 conjugate met many of its goals. The molecule was successfully synthesized, it binds mismatched DNA with high specificity and affinity, the hydrolysis of the platinum subunit allows for the platination of DNA, and along the way, an interesting interplay between photocleavage and platination was observed. However, the project faltered at its final goal: enhancing the differential antiproliferative effect of metalloinsertors with mismatch repair deficient cells. The reasons for this failure remain unclear. However, it may be that the RhPt2 conjugate was simply a little bit ahead of its time. All conceit aside, we have learned much about both the design of bifunctional conjugates and the cellular uptake of metal complexes since RhPt2 was first developed and tested. Thus, it may ultimately prove advantageous to revisit the idea of a metalloinsertor-platinum chemotherapeutic conjugate, for our newfound understanding of the issues of molecular design and uptake may tip the balance in favor of the successful combination of these two powerful families of molecules.

### 7.3: A METALLOINSERTOR CONJUGATE BEARING AN AUGER ELECTRON EMITTING

#### RADIONUCLIDE

##### 7.3.1: INTRODUCTION

Radiation therapy plays a central role in the treatment of cancer, and while external beam radiation and brachytherapy undoubtedly remain the most often employed modalities, interest in targeted radiopharmaceutical therapy has grown rapidly over the past three decades in both the laboratory and the clinic.<sup>45-49</sup>

$\beta$ -Emitters are the most commonly utilized radionuclides for therapeutic purposes, with their low linear energy transfer (LET,  $<0.2 \text{ keV}/\mu\text{m}$ )<sup>e</sup> and high range (100  $\mu\text{m}$  – 5 mm) making them particularly useful for the cross-fire irradiation of large tumors. Indeed, a number of  $\beta$ -emitting radionuclides are currently used in the clinic, including  $\text{Na}^{131}\text{I}$  for thyroid cancer,  $^{32}\text{PO}_4^{3-}$  for some blood cancers,  $^{89}\text{SrCl}_2$  for some bone cancers, and  $^{131}\text{I}$ -m-iodobenzylguanidine for neuroendocrine cancers.<sup>45</sup> However, while the low LET of  $\beta$ -emitting radionuclides makes them well-suited for large tumor masses, it can render them less effective at killing individual cancer cells. As a result, for some applications, the field is increasingly interested in  $\alpha$ -emitting radionuclides. Due to their short range (30–80  $\mu\text{m}$ ) and high LET (80–100  $\text{keV}/\mu\text{m}$ ),  $\alpha$ -emitters are tremendously cytotoxic to single cells and small tumors.<sup>50,51</sup> A large volume of work has centered on the labeling of monoclonal antibodies with  $\alpha$ -emitting nuclei; however, the progress has been somewhat limited by the small number of suitable radionuclides. Indeed, to date only  $^{211}\text{At}$ ,  $^{211}\text{Bi}$ , and  $^{213}\text{Bi}$  have been actively pursued, though new efforts at designing multi- $\alpha$ -emitting ‘nanogenerators’ are intriguing.<sup>52</sup>

---

<sup>e</sup> Linear energy transfer (LET) is the amount of energy lost per unit distance as an ionizing particle travels through a material. It depends on a given particle’s type, charge, and energy.

While most of the research into the development of targeted radiopharmaceuticals has centered on  $\alpha$ - and  $\beta$ -emitting nuclei, a third class of radionuclides has garnered increasing attention in recent years for its potential in DNA-targeted radiotherapeutic agents: Auger electron emitters. First discovered in the late 1920s by Pierre Auger, Auger electrons are low energy electrons ejected from radionuclides as a result of internal conversion or electron capture processes.<sup>53-55</sup> Indeed, almost half of all radionuclides emit Auger electrons (for a partial list, see **Figure 7.17**). The process is relatively simple (**Figure 7.18**). Taking  $^{111}\text{In}$  as an example, the radionuclide in question first undergoes an electron capture process that results in the emission of a  $\gamma$ -ray and the formation of an inner shell electron vacancy. An electron in a higher energy level then drops down to fill this hole, and the energy released during this conversion is transferred to another electron that is consequently ejected from the radionuclide. This ejected electron is an Auger electron. Interestingly, multiple Auger electrons, sometimes as many as 30, can be emitted per decay event. Returning to our model, after the ejection of the first Auger electron, there are now two vacancies, one created by the electron that filled the original hole and one formed by the ejection of the Auger electron. Now, the process repeats itself, with two electrons from higher energy orbitals filling these vacancies and two additional electrons ejected from the atom with the energy released upon these conversions. This process repeats itself in an Auger cascade until the vacancies reach the outermost energy levels. By this time, the radionuclide has emitted many Auger electrons and, as a result, has become a highly charged polycation. In an event provocatively named the Coulombic explosion, the polycation is neutralized by oxidizing the

Radionuclide	Half-Life (d)	Auger Yield	Total Energy (keV)
$^{51}\text{Cr}$	27.7	5.4	3.653
$^{55}\text{Fe}$	997.1	5.1	4.177
$^{67}\text{Ga}$	3.26	4.7	6.264
$^{75}\text{Se}$	120	7.4	5.74
$^{77}\text{Br}$	2.38	6.7	5.218
$^{99\text{m}}\text{Tc}$	0.25	4.0	0.899
$^{111}\text{In}$	2.8	14.7	6.75
$^{113\text{m}}\text{In}$	0.069	4.3	2.047
$^{115\text{m}}\text{In}$	4.5	6.1	2.847
$^{123}\text{I}$	0.55	14.9	7.419
$^{125}\text{I}$	60.1	24.9	12.241
$^{193\text{m}}\text{Pt}$	4.33	26.4	10.353
$^{195\text{m}}\text{Pt}$	4.02	32.8	22.526
$^{201}\text{Tl}$	3.04	36.9	15.273
$^{203}\text{Pb}$	2.16	23.3	11.63

**Figure 7.17. Some Auger-electron emitting radionuclides.** Note the considerable differences in Auger yield (the number of electrons emitted per decay), ranging from an average of 4.0 for  $^{99\text{m}}\text{Tc}$  to an average of 36.9 for  $^{201}\text{Tl}$ .<sup>56</sup>

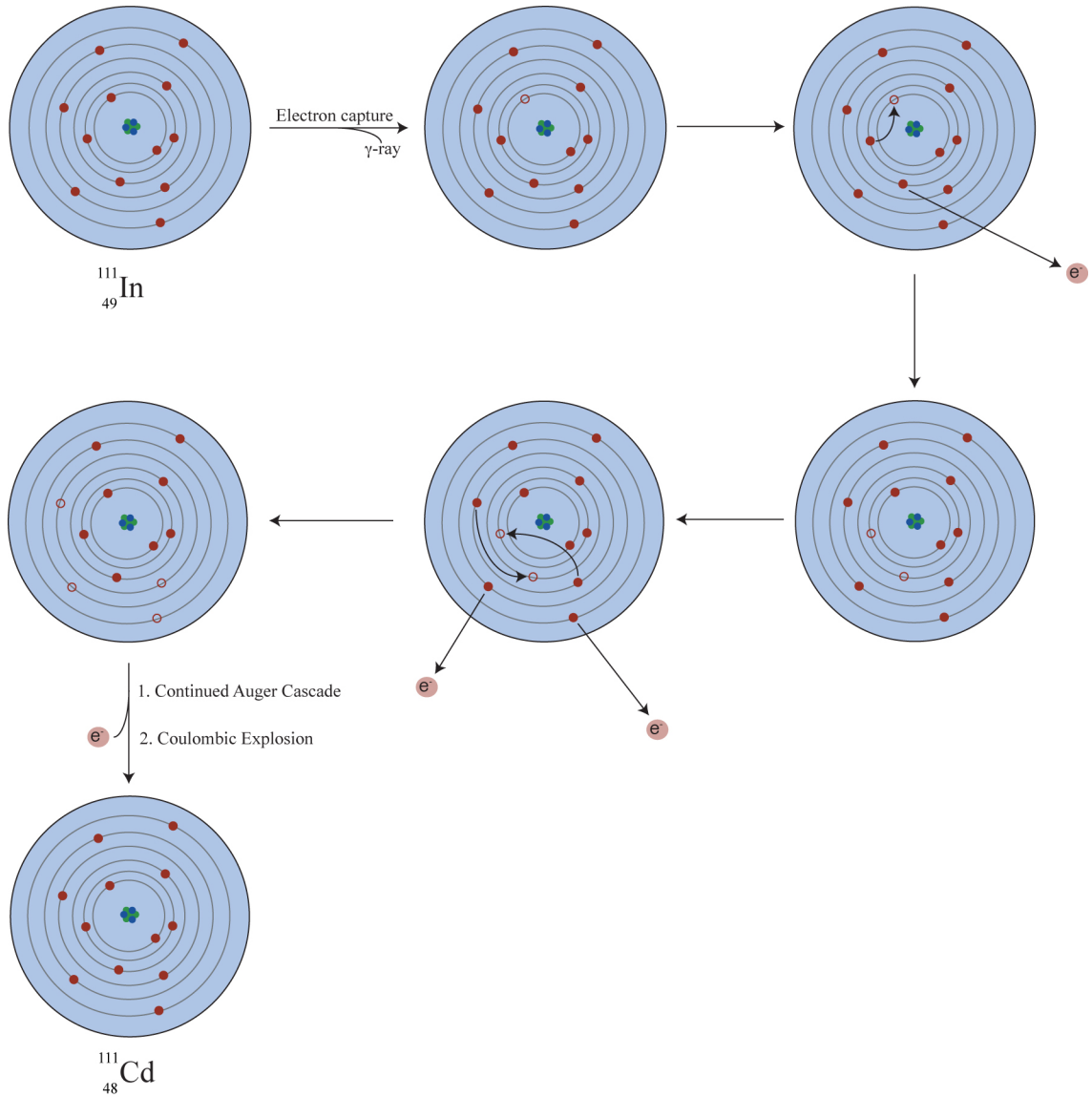


**Figure 7.18: Schematic of the Auger electron emission pathway of  $^{111}\text{In}$**

surrounding environment, forming the neutral daughter nucleus ( $^{111}\text{Cd}$  in the case of  $^{111}\text{In}$ ) and completing the process.

From a biomedical perspective, the high number of electrons per decay, high linear energy transfer (4–26 keV/ $\mu\text{m}$ ), and short path length (<20 nm in water) are the keys to the therapeutic potential of Auger electron emitters.<sup>56–58</sup> These three factors combine to create tremendous energy densities at, and only at, the site of decay. While this trait may limit the efficacy of these radionuclides in large tumors, it translates to extremely high cytotoxicity if the radionuclei are directed at the appropriate intracellular target, namely DNA. Indeed, if confined to the cytoplasm, an Auger electron emitting agent induces a cytotoxic response that follows a profile characteristic of low-LET radionuclides. If in the nucleus, however, the same agent will induce a cytotoxic response more characteristic of a very high LET radionuclide.<sup>57</sup>

From a mechanistic standpoint, Auger electrons promote cell death by both necrosis and radiation-induced apoptosis by creating double strand breaks in DNA.<sup>59, 60</sup> It is likely that reactive oxygen species created both by the Auger electrons themselves and the Coulombic explosion also play significant roles in mediating the biological effect. Further still, Auger electron emitters are largely non-toxic in the blood or near bone marrow and many undergo concomitant  $\gamma$ -decay that may allow for radiotherapy and diagnostic imaging with a single radionuclide.<sup>56, 57</sup> Given all this potential, it is not surprising that a number of Auger emitting therapeutic agents have been developed, including  $^{111}\text{In}$ -peptide conjugates<sup>61</sup>,  $^{125}\text{I}$ -labeled estrogens<sup>62</sup>,  $^{125}\text{I}$ - and  $^{123}\text{I}$ -labeled nucleosides<sup>63–65</sup>,  $^{195\text{m}}\text{Pt}$  transplatin<sup>66</sup>, and  $^{99\text{m}}\text{Tc}$ -intercalator conjugates<sup>67</sup> (**Figure 7.19**).

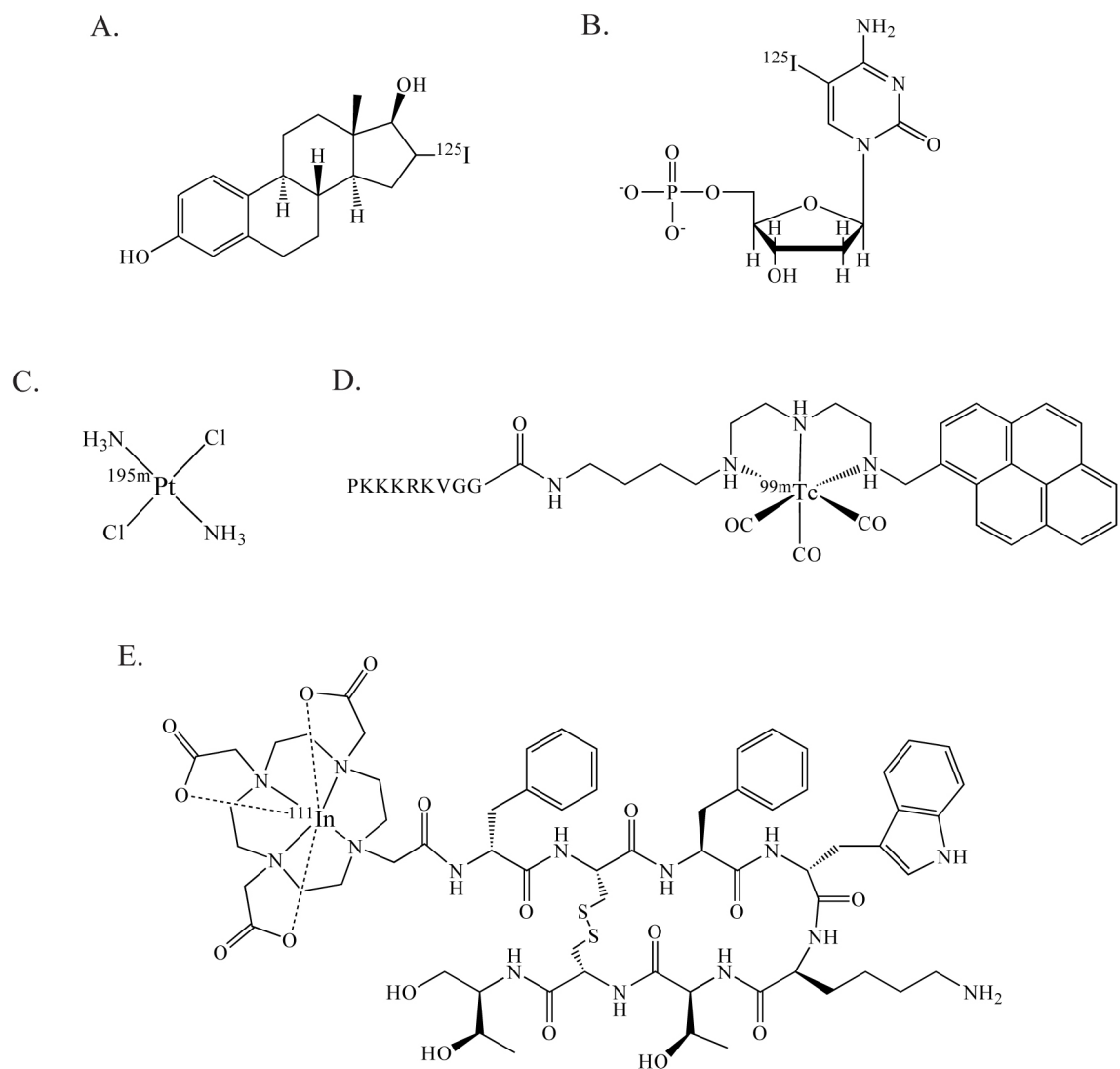


**Figure 7.19: Some Auger electron emitting radiotherapeutic agents.** (A)  $^{125}\text{I}$ -16- $\alpha$ -iodoestradiol<sup>62</sup>; (B) C5- $^{125}\text{I}$ -deoxycytosine<sup>63, 64</sup>; (C) *trans*- $^{195\text{m}}\text{Pt}(\text{NH}_3)_2(\text{Cl})_2$ <sup>66</sup>; (D) a  $^{99\text{m}}\text{Tc}$ -nuclear localization signal-pyrene conjugate<sup>67</sup>; (E)  $^{111}\text{In}$ -Octreotide, a clinically-employed,  $\gamma$ -emitting imaging agent that is currently being investigated for its efficacy as a Auger-emitting radiotherapeutic.<sup>61</sup>

The mismatch-specific conjugates previously developed by our laboratory for therapeutic applications have undeniably proven successful in oligonucleotide-based experiments.<sup>12, 13</sup> However, their *in vivo* success at preferentially inhibiting the proliferation of mismatch repair deficient cells has been limited. This is likely because the differential antiproliferative activity of these conjugates is predicated on their selective accumulation in mismatch repair deficient cells. For example, because the alkylator subunit of the metalloinsertor-nitrogen mustard conjugate is cytotoxic whether the rhodium subunit is bound to DNA or not, we must rely on the mismatch-specific binding of the metalloinsertor to lead to the selective accumulation of the conjugate in mismatch repair deficient cells.<sup>12</sup> This is a departure from the principles behind the biological activity of  $\text{Rh}(\text{bpy})_2(\text{chrysi})^{3+}$  and  $\text{Rh}(\text{bpy})_2(\text{phzi})^{3+}$ . While the exact mechanistic details are still murky, it has become abundantly clear that the differential biological effect of these complexes is based on their specific binding of DNA mismatches.<sup>8, 9</sup> It follows, then, that the selective accumulation of these complexes in MMR-deficient cells is likely a minor factor, if one at all, in the observed differential effect. This supposition is further supported by recent ICP-MS experiments that show no differential accumulation of rhodium in MMR-proficient and -deficient cells.

Auger electron emitting radionuclides afford a singular opportunity to create bifunctional metalloinsertor conjugates with antiproliferative effects that are based on specific binding of mismatched DNA rather than selective localization in MMR-deficient cells. Because of the unique properties of Auger electrons, Auger electron emitting radionuclides are only capable of producing a significant cytotoxic response if *bound* to DNA. Importantly, simply being in the nucleus is not good enough. Investigations have

shown that DNA-bound Auger emitters kill cells far more efficiently than nucleus-localized, but non-DNA-bound emitters. The ramifications for a mismatch-specific, bifunctional conjugate are clear. In MMR-deficient cells, the Rh-Auger conjugate will enter the nucleus, bind to mismatches in the DNA, cause double strand breaks upon decay, and prompt cell death. In MMR-proficient cells, the Rh-Auger conjugate will still enter the nucleus, but in this case, the absence of mismatches will prevent DNA binding, and thus the conjugate will be far less effective at killing the cells (**Figure 7.20**). Clearly, a Rh-Auger conjugate holds tremendous potential as a selective cytotoxic agent for mismatch repair deficient cells.

Herein, we present preliminary investigations into the design, synthesis, and study of a mismatch-specific, metalloinsertor-Auger electron emitter conjugate.

### **7.3.2: DESIGN**

The most important design decision in the development of a Rh-Auger conjugate is the choice of radionuclide. The ultimate goal of this line of investigation is, of course, the development of a therapeutic agent. Thus, it was tempting to choose one of the more clinically applicable Auger emitting radionuclides, such as  $^{111}\text{In}$ ,  $^{123}\text{I}$ , or  $^{99\text{m}}\text{Tc}$ . However, many other preliminary investigations have employed a different radionuclide,  $^{125}\text{I}$ , in proof-of-concept model systems. Granted, the 60-day half-life of  $^{125}\text{I}$  renders it relatively unusable for clinical applications. However, it is often employed in this manner primarily because  $^{125}\text{I}$  has been shown to promote double strand breaks particularly well, most likely a result of its high number of Auger electrons emitted per decay, and thus

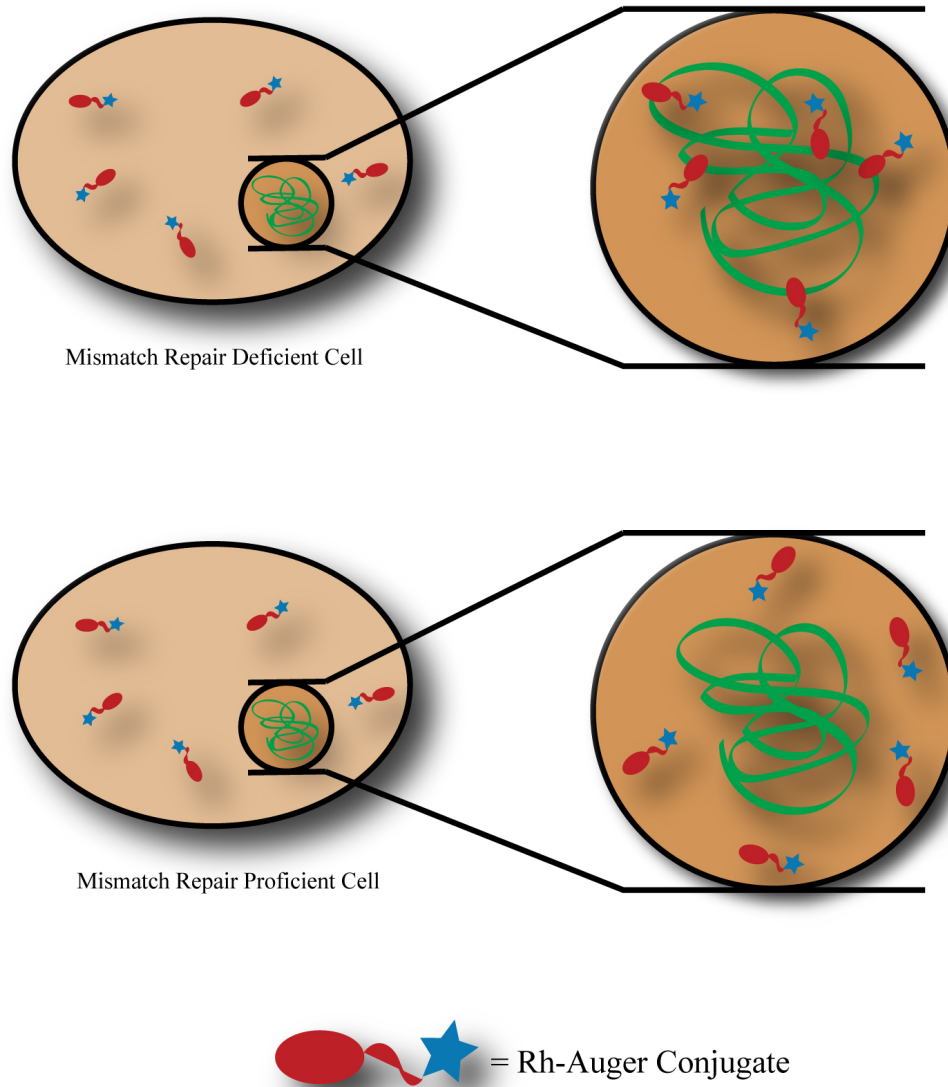


**Figure 7.20: A Rh-Auger conjugate in MMR-proficient and -deficient cells.** In MMR-deficient cells, the Rh-Auger conjugate will enter the nucleus, bind to mismatches in the DNA, cause double strand breaks upon decay, and prompt cell death. In MMR-proficient cells, the Rh-Auger conjugate will still enter the nucleus, but in this case, the absence of mismatches will prevent DNA-binding, and thus the conjugate will be far less effective at killing the cells.

lends itself well to PAGE electrophoresis studies with radiolabeled oligonucleotides.<sup>63, 64,</sup>  
<sup>68</sup> The well-developed chemistry of iodination reactions may also play a significant role in the frequency of <sup>125</sup>I use. At bottom, if a Rh-<sup>125</sup>I conjugate proves successful in oligonucleotide experiments, a new, more clinically relevant radionuclide such as <sup>111</sup>In or <sup>123</sup>I can be substituted with relative ease.

### 7.3.3: SYNTHESIS

The exigencies of radiochemistry required that this conjugate be synthesized in a linear fashion, with the <sup>125</sup>I radionuclide introduced last. Based on the structure considerations discussed earlier in this chapter, a trisheteroleptic metalloinsertor bearing a dipyridylamine ligand with a carboxy-terminated linker was employed. The metalloinsertor-linker subunit was synthesized in a step-wise fashion from RhCl<sub>3</sub> (**Figure 7.21**). The radioiodination reaction requires a phenolic hydroxyl group for substitution with <sup>125</sup>I.<sup>69</sup> Therefore, a tyramine was then coupled to the metalloinsertor subunit using HATU to provide the necessary radioiodination substrate. Next, the Rh-tyramine conjugate was purified by cation exchange chromatography and HPLC and sent to Perkin-Elmer for radioiodination. After one week, the radiolabeled and HPLC-purified Rh-<sup>125</sup>I conjugate was returned (**Figure 7.22**). The specific activity of the final product was 2200 Ci/mmol (2070 μCi/μg), and it was provided at a concentration of 250 μCi/mL (120 nM Rh). The initial radiochemical purity of the Rh-<sup>125</sup>I conjugate was >95%.

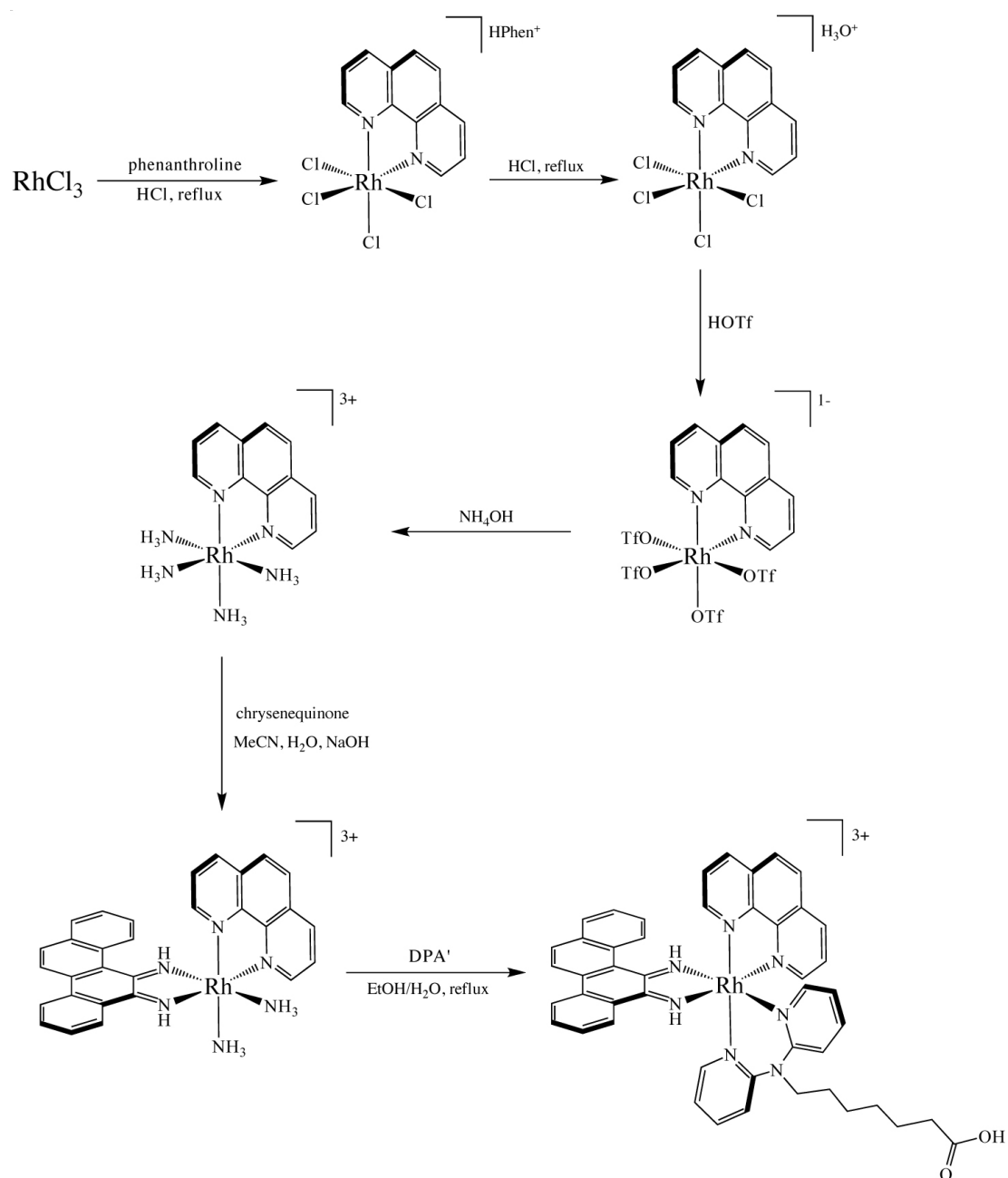


**Figure 7.21. The synthetic route to the trisheteroleptic metalloinsertor subunit.** The conjugate's metalloinsertor subunit was synthesized via the sequential addition of phen, chrysi, and  $\text{DPA}'$  ligands to a rhodium center.

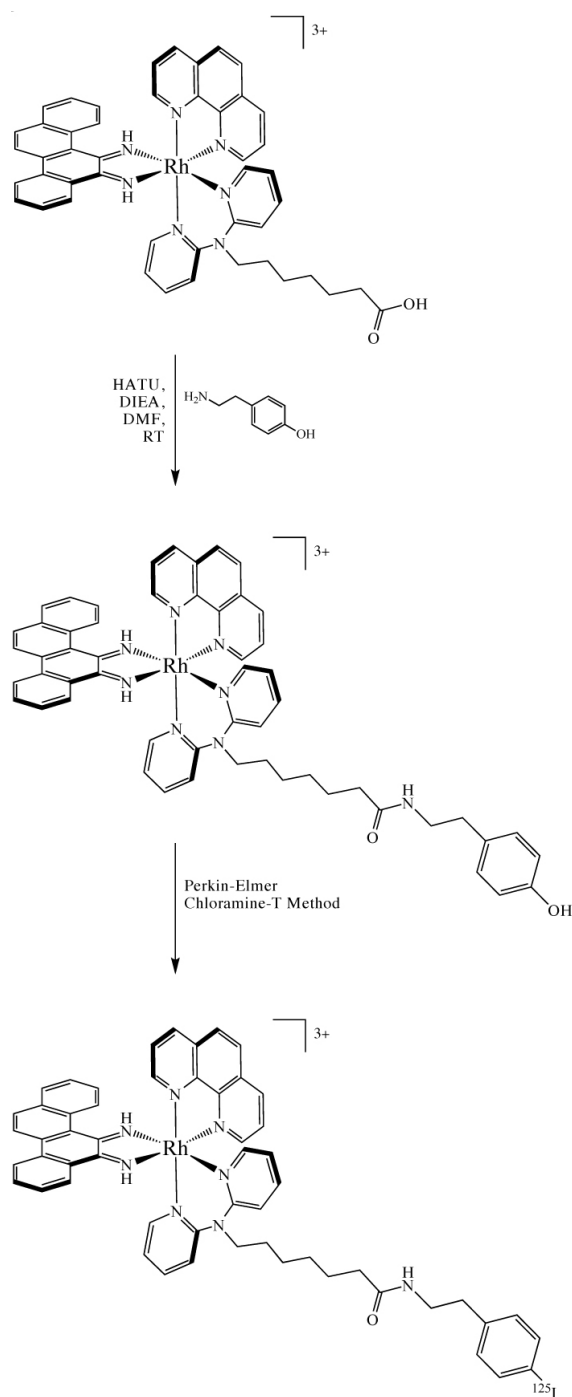


**Figure 7.22: The synthetic route to Rh-<sup>125</sup>I.** Tyramine was first coupled to the metalloinsertor subunit to provide a hydroxyl group for the labeling reaction. Then, the completed Rh-tyramine conjugate was sent to Perkin-Elmer for radioiodination via the Chloramine-T method.<sup>69</sup>

#### 7.3.4: DNA CLEAVAGE STUDIES

In order to interrogate the mismatch-specific binding and photocleavage of the Rh-<sup>125</sup>I experiment, the precursor Rh-tyramine conjugate was employed in denaturing PAGE experiments using 5'-<sup>32</sup>P-labeled oligonucleotides containing or lacking a central C•C mismatch. These experiments illustrate that the Rh-tyramine conjugate (and, by proxy, the Rh-<sup>125</sup>I conjugate) specifically recognizes mismatched DNA (**Figure 7.23**). Due to the substitution of a linker-modified dipyrindylamine for the linker-modified bipyridine ligand, the Rh-tyramine conjugate displays considerably reduced photocleavage efficiency. This loss in photochemistry, however, is inconsequential for the radionuclide conjugates, for in this case, the job of the metalloinsertor unit is simply to bind mismatch DNA and bring the radionuclide moiety in close proximity to the helix.

Next, preliminary PAGE experiments were performed to investigate the Auger electron mediated DNA cleavage of Rh-<sup>125</sup>I with matched and mismatched oligonucleotides. For these experiments, 5  $\mu$ L solutions of Rh-<sup>125</sup>I (60 nM Rh, 1.25  $\mu$ Ci) were combined with equal volume solutions of 5'-<sup>32</sup>P-labeled oligonucleotides containing a central C•G, C•C, or C•A base pair (50, 100, or 150 nM). The samples were frozen to prevent diffusion of reactive oxygen species and incubated for two, three, or four weeks. Autoradiography of the resultant gels shows little cleavage in any of the DNA strands after 7, 14, or 21 days of incubation (**Figure 7.24**). This is somewhat surprising, considering the conjugate is known to bind selectively to mismatched DNA, and this would almost certainly bring the radionuclide in close enough proximity to the duplex to promote strand scission.

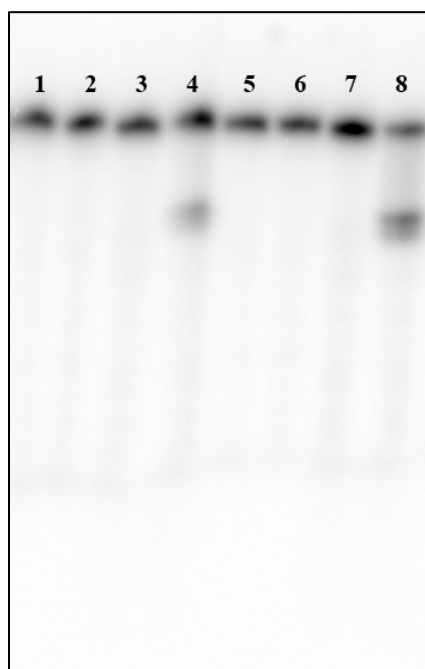


**Figure 7.23: Mismatch recognition and photocleavage by Rh-tyramine.**

Autoradiogram of a denaturing 20% polyacrylamide gel showing the mismatch recognition and photocleavage of Rh-tyramine. Conditions are duplex (1  $\mu$ M) and Rh complex (1  $\mu$ M) in 20 mM NaCl, 10 mM NaPi, pH 7.1. Irradiations were performed using an Oriel Instrument Solar Simulator (320–440 nm). Lane 1: matched DNA, light control. Lane 2: matched DNA, Rh-Tyr, 15 min irradiation. Lane 3: mismatched DNA, light control. Lane 4: mismatched DNA, Rh-Tyr, 15 min irradiation. Lane 5: matched DNA, light control. Lane 6: matched DNA, Rh(bpy)<sub>2</sub>(chrysi)<sup>3+</sup>, 15 min irradiation. Lane 7: mismatched DNA, light control. Lane 8: mismatched DNA, Rh(bpy)<sub>2</sub>(chrysi)<sup>3+</sup>, 15 min irradiation. The DNA sequence is 5'-<sup>32</sup>P-GAC CAG CTT ATC ATC CCT AGA TTA GCG-3' where the bold, red C is complementary to another C in the mismatched duplexes and a G in the matched duplexes.

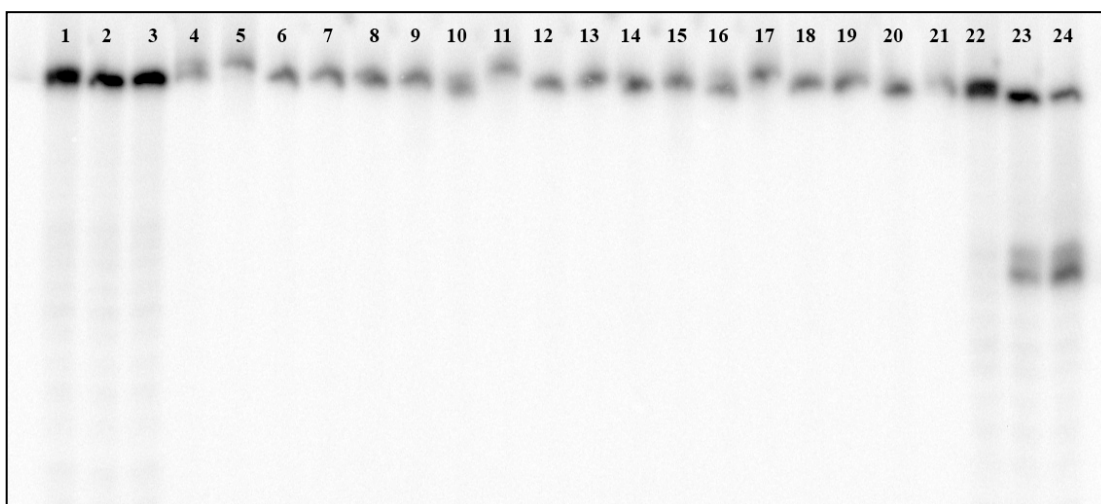


**Figure 7.24: DNA cleavage of Rh-<sup>125</sup>I.** Autoradiogram of a denaturing 20% polyacrylamide gel showing DNA cleavage properties of Rh-<sup>125</sup>I. Conditions are duplex (50, 100, or 150 nM) and Rh complex (60 nM, 1.25  $\mu$ Ci) in 20 mM NaCl, 10 mM NaPi, pH 7.1. Incubations are for 21 days at -80 °C. The forward (F) strand DNA sequence is 5'-GAC CAG CTT ATC ATC CCT AGA TTA GCG-3'. The matched sequence (M) is 5'-CGC TTA TCT AGG GAT GAT AAG CTG GTC-3'. The C•A mismatched sequence (A) is 5'-CGC TTA TCT AGG AAT GAT AAG CTG GTC-3'. The C•C mismatched sequence (C) is 5'-CGC TTA TCT AGG CAT GAT AAG CTG GTC-3'. For each assembly, lanes were run with each strand labeled in order to check for double strand breaks. Thus, F\*M denotes matched DNA with the forward strand labeled. Lanes 1, 2, and 3 contain dark control experiments with 100 nM F\*M, F\*A, and F\*C, respectively. Lanes 4, 10, and 16 contain F\*M DNA. Lanes 5, 11, and 17 contain FM\* DNA. Lanes 6, 12, and 18 contain F\*A DNA. Lanes 7, 13, and 19 contain FA\* DNA. Lanes 8, 14, and 20 contain F\*C DNA. Lanes 9, 15, and 21 contain FC\* DNA. Lanes 22, 23, and 24 contain Rh(bpy)<sub>2</sub>(chrysi)<sup>3+</sup> photocleavage experiments with 100 nM F\*M, F\*A, and F\*C, respectively. Irradiations were performed using an Oriel Instrument solar simulator (320–440 nm).

A few different factors may be at the root of these results. It is possible that the aliphatic linker and tyramine moiety simply move the radionuclide too far away from the DNA, out of the effective range of the Auger electrons. This, however, is not likely, because the  $^{125}\text{I}$  lies only thirteen bonds from the dipyridylamine ligand, and even this distance, which assumes a fully extended linker, is within the range of most Auger electrons. A more likely explanation lies in the low specific activity (1.25  $\mu\text{Ci}$ ) of the conjugates employed in the Auger electron DNA cleavage experiments. Indeed, other laboratories typically employ specific activities almost two orders of magnitude higher (~70–100  $\mu\text{Ci}$ ) for similar experiments.<sup>63, 64, 68</sup> This issue will be difficult to remedy in the current experimental environment. Because Perkin-Elmer typically performs  $^{125}\text{I}$ -iodinations for imaging applications (which require lower specific activities), the 250  $\mu\text{Ci/mL}$  with which they provided our laboratory was the maximum specific activity at which they label. Normally, the solution of radiolabeled conjugate could simply be concentrated *in vacuo*, but our laboratory is not a radiochemistry laboratory, and the Environmental Health and Safety Office strongly discourage using common laboratory equipment in conjunction with the  $^{125}\text{I}$ -labeled conjugate.

### 7.3.5: CONCLUSION

The idea of metalloinsertor-Auger electron emitter conjugate is certainly a work in progress. The principle is sound. In a seminal paper on the topic, O'Donoghue and Whelton distill the issue quite nicely: “For an Auger-targeting therapy based on [DNA-binding], biological specificity would rely on the existence of qualitative or quantitative differences in DNA sequence between tumor and normal cells.”<sup>58</sup> This is precisely the

case in mismatch repair deficient tumors. Further still, mismatch-specific metalloinsertors provide a means to bring Auger electron emitting radionuclides into close range of the DNA of MMR-deficient cells while allowing them to stay at a safer distance from that of MMR-proficient cells.

The Rh-<sup>125</sup>I conjugate described herein may well provide a proof-of-concept model for this system. To be sure, changes in our radiochemical setup and procedures will be necessary for success and design changes to bring the metalloinsertor and radionuclide moieties closer together may be advisable. Further, a conjugate with a more clinically applicable radionuclide, such as <sup>111</sup>In or <sup>123</sup>I, will need to be adopted for any future *in vitro* and *in vivo* studies. Ultimately, while it is certain that there is much left to be done, mismatch-specific, Auger electron emitting conjugates hold tremendous potential for the treatment of mismatch repair deficient tumors and will hopefully merit further attention from our laboratory.

#### 7.4: EXPERIMENTAL PROTOCOLS

Many of the procedural details for this investigation are included in Chapter 2 of this text. These include the following: the syntheses of Rh(phen)(chrysi)(NH<sub>3</sub>)<sub>2</sub><sup>3+</sup> (2.3.4.1–2.3.4.5), <sup>NH2</sup>bpy (2.3.5.1–2.3.5.3), and DPA' (2.3.5.7, 2.3.5.10, 2.3.5.11), Rh(phen)(chrysi)(<sup>NH2</sup>bpy)<sup>3+</sup> (by analogy to 2.3.5.12), and Rh(phen)(chrysi)(DPA')<sup>3+</sup> (2.3.5.13); the synthesis, purification, and radiolabeling of oligonucleotides (2.4.1–2.4.2); the Maxam-Gilbert sequencing of radiolabeled DNA (2.4.3); and the performance of recognition and binding titration experiments via PAGE (2.4.4.1–2.4.4.2).

#### 7.4.1: MATERIALS AND INSTRUMENTATION

All reagents were obtained from commercial sources and used as received without further purification.  $\text{RhCl}_3$  was purchased from Pressure Chemicals.  $\text{K}_2\text{PtCl}_4$  was purchased from Strem Chemicals. Media and supplements were purchased from Invitrogen. BrdU, antibodies, buffers, and peroxidase substrate were purchased in kit format from Roche Molecular Biochemicals. Radioiodination was performed by Perkin-Elmer. All non-aqueous solvents were purchased from Fluka and stored under argon and over molecular sieves. All water used was purified using a MilliQ water purification system. Unless otherwise noted, all reactions were performed under ambient conditions.

$^1\text{H-NMR}$  spectra were recorded on a Varian 300 MHz spectrometer at room temperature using solvent residual signal as a reference to TMS. Mass spectrometry was performed at either the Caltech mass spectrometry facility or in the Beckman Institute Protein/Peptide Micro Analytical Laboratory (PPMAL). Absorption spectra were recorded on a Beckman DU 7400 spectrophotometer. Extinction coefficients were determined using inductively coupled plasma mass spectrometry (ICP-MS).

Oligonucleotides were synthesized on an ABI 3400 DNA synthesizer and purified via HPLC in duplicate (DMT-off and DMT-on) before use. All reverse-phase HPLC purifications were performed on an HP1100 high-pressure liquid chromatography system equipped with diode array detector using a Varian DynaMax C18 semipreparative column (see Chapter 2, Section 2.4.1). Irradiations were performed using an Oriel Instruments solar simulator (320–440 nm). All PAGE experiments described employed denaturing 20% polyacrylamide gels (SequaGel, National Diagnostics) and were performed according to published procedures. Further, gels were developed using

Molecular Dynamics phosphorimaging screens and a Molecular Dynamics Storm 820 phosphorimager and were subsequently visualized and quantified with Molecular Dynamics ImageQuant software.

#### **7.4.2: SYNTHESIS AND TESTING OF RHPT2**

##### **7.4.2.1: SYNTHESIS OF 4-FORMYLBENZOIC ACID TERT-BUTYL ESTER (METHOD 1)**

In a 50 mL round-bottom flask, 1.30 g 4-carboxybenzaldehyde (8.7 mmol) were suspended in benzene (15 mL, dry) and brought to reflux under argon. Still under argon, 4.5 mL N,N-dimethyldi-tert-butylacetal (18.8 mmol, 2.2 equiv) were added dropwise over the course of 15 min. The reaction was monitored via TLC (SiO<sub>2</sub>, CH<sub>2</sub>Cl<sub>2</sub>). After 3 h, the yellow reaction mixture was allowed to cool to room temperature, extracted with NaHCO<sub>3</sub>(aq), washed with brine, dried with MgSO<sub>4</sub>, and concentrated via rotary evaporation. The residue was purified via column chromatography (SiO<sub>2</sub>, 5:1 hexanes:diethyl ether) to yield 1.1 g of the product as a yellow oil (61%).

<sup>1</sup>H-NMR (CDCl<sub>3</sub>): 10.11 ppm (s, 1H); 8.17 ppm (d, 2H); 7.94 ppm (d, 2H), 1.66 ppm (s, 9H).

##### **7.4.2.2: SYNTHESIS OF 2-(4-TERT-BUTOXYCARBONYLBENZYLIDENE)-MALONIC ACID DIBENZYL ESTER (METHOD 1)**

In a 10 mL round-bottom flask, 500 mg 4-formylbenzoic acid tert-butyl ester (2.4 mmol) and 0.62 mL dibenzylmalonate (2.5 mmol, 1 equiv.) were dissolved in dry THF (3 mL) and cooled down in an ice bath. Then, 0.56 mL titanium tetrachloride (5 mmol, 2 equiv.) were added, and the mixture was stirred under argon at 0 °C for 3 h. After 3 h, 0.8

mL dry pyridine were added, and the mixture was warmed to room temperature and stirred for 48 h. After 48 h, water (20 mL) and dichloromethane (50 mL) were added to the reaction mixture. The organic layer was separated, extracted three more times with dichloromethane, washed with brine, dried with MgSO<sub>4</sub>, and concentrated via rotary evaporation. The residue was purified via column chromatography (SiO<sub>2</sub>, CH<sub>2</sub>Cl<sub>2</sub>) to yield 550 mg of the product as a white solid (47%).

<sup>1</sup>H-NMR (CDCl<sub>3</sub>): 7.83 ppm (d, 2H); 7.79 ppm (s, 1H); 7.25-7.45 ppm (m, 12H), 5.29 ppm (s, 2H), 5.26 ppm (s, 2H), 1.62 ppm (s, 9H).

ESI-MS: 473 [M+H]<sup>+</sup>

#### **7.4.2.3: SYNTHESIS OF 2-(4-CARBOXYBENZYLIDENE)-MALONIC ACID DIBENZYL ESTER (METHOD 2)**

In 10 mL round-bottom flask, 1.9 g 4-carboxybenzaldehyde (12.7 mmol) and 3.2 mL dibenzylmalonate (12.7 mmol, 1 equiv.) were cooled in an ice bath. Dry carbon tetrachloride (5 mL) and 2.5 mL titanium tetrachloride (1.8 equiv.) were then added to the reaction mixture under argon. The yellow mixture was stirred at 0 °C for 3 h. After 3 h, 4 mL dry pyridine were added, and the mixture was warmed to room temperature and stirred for 48 h. After 48 h, water (20 mL) and dichloromethane (50 mL) were added to the reaction mixture. The organic layer was separated, extracted three more times with dichloromethane, washed with brine, dried with MgSO<sub>4</sub>, and concentrated via rotary evaporation to yield a yellow oil. The oil was then triturated with diethyl ether, and the resultant white solid was filtered and air dried to produce 3.2 g of the desired product (61%).

$^1\text{H-NMR}$  ( $\text{CDCl}_3$ ): 7.96 ppm (d, 2H); 7.81 ppm (s, 1H); 7.25–7.45 ppm (m, 12H), 5.29 ppm (s, 2H), 5.27 ppm (s, 2H).

ESI-MS: 417  $[\text{M}+\text{H}]^+$

#### **7.4.2.4: SYNTHESIS OF 2-(4-TERT-BUTOXYCARBONYLBENXYLIDENE)-MALONIC ACID DIBENZYL ESTER (METHOD 2)**

In a 250 mL round-bottom flask, 3.58 g 2-(4-carboxbenzylidene)-malonic acid dibenzyl ester (8.6 mmol) were suspended in  $\text{CH}_2\text{Cl}_2$ , and 4 drops of neat sulfuric acid were added to the solution. Under argon, isobutene was bubbled through the solution for 5 min. The suspension was stirred under argon at room temperatures for 3 days, and isobutene was bubbled through the solution every 7 h. After 3 days, the mixture was diluted with  $\text{CH}_2\text{Cl}_2$  (50 mL) and saturated  $\text{NaHCO}_3$  (aq) (50 mL) and shaken in a separatory funnel, and the organic layer was isolated. The aqueous layer was then further extracted with  $\text{CH}_2\text{Cl}_2$  (3 x 50 mL). The combined organic layers were washed with brine, dried with  $\text{MgSO}_4$ , and concentrated via rotary evaporation to yield 4.0 g of the product as a colorless oil that solidifies to a white solid with time (>98%). The  $^1\text{H-NMR}$  and ESI-MS were identical to those obtained for the product of the reaction described in Section 7.4.2.2.

#### **7.4.2.5: SYNTHESIS OF 2-(4-TERTBUTOXYCARBONYLBENZYL)-MALONIC ACID**

In a 50 mL Schlenk flask, 40 mg 10% Pd/C were added to 300 mg 2-(4-tert-butoxycarbonylbenzylidene)-malonic acid dibenzyl ester in 15 mL of EtOH. The reaction vessel was evacuated, filled with  $\text{H}_{2(\text{g})}$ , and stirred overnight. After 16 h, the reaction

mixture was opened to the atmosphere and filtered through celite. The resultant solution was concentrated via rotary evaporation to yield 180 mg of the product as a thick colorless oil (>95%).

$^1\text{H-NMR}$  ( $\text{CDCl}_3$ ): 7.92 ppm (d, 2H); 7.28 ppm (d, 2H); 3.74 ppm (t, 1H), 3.31 ppm (d, 2H), 1.57 ppm (s, 9H).

ESI-MS: 295  $[\text{M}+\text{H}]^+$

#### 7.4.2.6: SYNTHESIS OF $\text{Pt}(\text{DACH})\text{I}_2$

In a 50 mL round-bottom flask, 1.0 g  $\text{K}_2\text{PtCl}_4$  (2.40 mmol) was dissolved in water (10 mL) by heating to 50 °C. An aqueous solution of 1.95 g KI in 4 mL water (11.7 mmol, 5 equiv.) was then added dropwise to the reaction mixture, and the dark brown solution was allowed to stir at 50 °C for 10 min. After 10 min, a solution of 0.3 g 1R,2R-(-)-transdiaminocyclohexane (dach) in 3 mL water (2.6 mmol, 1.1 equiv.) was added dropwise to the solution. A dark yellow precipitate then formed nearly immediately, and after 30 min more stirring, the precipitate was centrifuged, washed with water (3 x 10 mL) and cold ethanol (1 x 5 mL), and dried *in vacuo* to yield 1.32 g of the product as a dark yellow solid (98%).

#### 7.4.2.7: SYNTHESIS OF $\text{Pt}(\text{DACH})(\text{NO}_2)_2$

In a 50 mL round-bottom flask, 500 mg  $\text{Pt}(\text{dach})(\text{I})_2$  and 300 mg  $\text{AgNO}_3$  (1.83 mmol, 2 equiv.) were suspended in water (20 mL). The resultant mixture was then protected from light and stirred at 60 °C for 30 min. After 30 min, a beige precipitate had formed. This precipitate was filtered and washed with water (2 x 5 mL). The resultant

clear filtrate was checked for silver (dilute HCl), concentrated *in vacuo*, taken up in water (20 mL), and filtered through celite. The filtrate was then concentrated again *in vacuo* and triturated in a mixture of methanol (8 mL) and water (0.1 mL). The off-white residue was filtered, washed with methanol, and dried again *in vacuo* to yield 290 mg of the product as a white solid (70%).

$^1\text{H-NMR}$  ( $\text{CDCl}_3$ ): 7.92 ppm (d, 2H); 7.28 ppm (d, 2H); 3.74 ppm (t, 1H), 3.31 ppm (d, 2H), 1.57 ppm (s, 9H).

ESI-MS: 295  $[\text{M}+\text{H}]^+$

#### **7.4.2.8: SYNTHESIS OF $\text{Pt}(\text{DACH})(\text{MALBzCOOtBu})$**

In a 50 mL round-bottom flask, 120 mg  $\text{Pt}(\text{dach})(\text{NO}_2)_2$  were dissolved in water (15 mL) via sonicating and heating. A solution of 90 mg 2-(4-tertbutoxycarbonylbenzyl)-malonic acid (1.1 equiv.) in 5 mL 0.12 M KOH was then added dropwise to the platinum solution at room temperature over the course of 5 min. The resultant mixture was then stirred at 50 °C for 3 h. After 3 h, the mixture was chilled to 4 °C in the cold room and left there over night. The next morning, a white solid had formed and was filtered, washed with water (5 mL) and diethyl ether (5 mL), and dried *in vacuo* to yield 100 mg of the desired product as an off-white powder (60%).

$^1\text{H-NMR}$  ( $\text{CD}_3\text{OD}$ ): 7.84 ppm (d, 2H); 7.39 ppm (d, 2H); 4.14 ppm (t, 1H), 3.43 ppm (d, 2H), 2.25–2.35 ppm (m, 2H), 1.9–2.1 ppm (m, 2H), 1.4–1.6 ppm (m, 11H), 1.1–1.4 (m, 4H).

ESI-MS: 602  $[\text{M}+\text{H}]^+$

#### 7.4.2.9: SYNTHESIS OF Pt(DACH)(MALBzCOOH)

In a 10 mL round-bottom flask, 100 mg Pt(dach)(MalBzCOOtBu) were dissolved in 1.5 mL neat TFA and warmed to 35 °C for 5 min. After 5 min, the TFA was removed *in vacuo*, and the resultant pale yellow solid was washed with 5 mL diethyl ether by suspension, centrifugation, and removal of the supernatant. After 10 repeated rounds of washing, the pale yellow solid was air-dried to produce the 50 mg of the desired product as a grey solid (60%).

<sup>1</sup>H-NMR (d<sub>6</sub>-DMSO): 7.82 ppm (d, 2H); 7.31 ppm (d, 2H); 7.0–6.3 ppm (broad m, 2H), 6.1–5.8 ppm (broad m, 2H), 5.4–5.0 ppm (broad m, 2H), 4.02 ppm (t, 1H), 3.08 ppm (d, 2H), 2.20–1.70 ppm (m, 4H), 1.5–0.9 ppm (m, 6H).

ESI-MS: 545 [M+H]<sup>+</sup>

#### 7.4.2.10: SYNTHESIS OF RHPT2

In a flame-dried, Argon-filled 10 mL Schlenk flask, Pt(dach)(MalBzCOOH) (25 mg) and Rh(phen)(chrysi)(<sup>NH<sub>2</sub></sup>bpy)<sup>3+</sup> (5 mg) were dissolved in 2 mL DMF. The resultant vessel was purged with Ar<sub>(g)</sub> for 5 minutes and then stirred for 2 h at room temperature. After 2 h, 0.5 mL DIEA was added, and the resultant reaction mixture was allowed to stir overnight under argon. After 16 h, H<sub>2</sub>O (4 mL) was added to the reaction mixture, and the aqueous solution was loaded onto a C18 reverse-phase cartridge (Waters Sep-Pak), washed with water, and eluted with 1:1:0.001 (H<sub>2</sub>O:MeCN:TFA). The purified product was frozen and lyophilized to dryness. Each conjugate was further purified via reverse-phase high-performance liquid chromatography using an HP1100 HPLC system, a Varian

DynaMax C18 semipreparative column, and an elution gradient of 85:15 to 40:60 H<sub>2</sub>O (0.1% TFA):MeCN (0.1% TFA) over 60 min.

ESI-MS: 674 [M-H]<sup>2+</sup>, 1347 [M-2H]<sup>+</sup>

UV-Vis (H<sub>2</sub>O, pH 7.0):  $\lambda_{\max}$  267 nm ( $\epsilon = 68,000 \text{ M}^{-1}$ ), 301 nm ( $\epsilon = 40,000 \text{ M}^{-1}$ ), 313 nm ( $\epsilon = 30,400 \text{ M}^{-1}$ ), 389 nm ( $\epsilon = 19,400 \text{ M}^{-1}$ ).

#### **7.4.2.11: PLATINATION PAGE EXPERIMENTS**

The platination PAGE experiments with radiolabeled DNA were performed according to the protocols described for recognition and photocleavage experiments in Chapter 2 Section 2.4.4.1. The only difference here is that in many cases, the samples were permitted to incubate for extended periods of time.

#### **7.4.2.12: CELL CULTURE**

HCT116N and HCT116O cells were grown in RPMI medium 1640 supplemented with 10% FBS, 2 mM L-glutamine, 0.1 mM nonessential amino acids, 1 mM sodium pyruvate, 100 units/mL penicillin, 100  $\mu\text{g/mL}$  streptomycin, and 400  $\mu\text{g/mL}$  Geneticin (G418). Cells were grown in tissue culture flasks and dishes (Corning Costar) at 37 °C under 5% CO<sub>2</sub> atmosphere.

#### **7.4.2.13: CELLULAR PROLIFERATION ELISA**

HCT116N and HCT116O cells were plated in 96-well plates at 2000 cells/well and allowed 24 h to adhere. The cells were then incubated with the metal complexes of interest for 24 h. After 24 h the metal-containing medium was replaced with fresh

medium, and the cells were allowed to grow for 48 more h. Cells were labeled with BrdU 24 h before analysis. The amount of BrdU incorporation was quantified by antibody assay according to established procedures. Cellular proliferation was expressed as the ratio of the amount of BrdU incorporated by the treated cells to that of the untreated cells.

### **7.4.3: SYNTHESIS OF TESTING OF RH-<sup>125</sup>I**

#### **7.4.3.1: SYNTHESIS OF RH-TYRAMINE**

In a flame-dried, Argon-filled 10 mL Schlenk flask tyramine (25 mg) and Rh(phen)(chrysi)(DPA')<sup>3+</sup> (5 mg) were dissolved in 2 mL DMF. The resultant vessel was purged with Ar<sub>(g)</sub> for 5 min and then stirred for 2 h at room temperature. After 2 h, 0.5 mL DIEA were added, and the resultant reaction mixture was allowed to stir overnight under argon. After 16 h, H<sub>2</sub>O (4 mL) was added to the reaction mixture, and the aqueous solution was loaded onto a C18 reverse-phase cartridge (Waters Sep-Pak), washed with water, and eluted with 1:1:0.001 (H<sub>2</sub>O:MeCN:TFA). The purified product was frozen and lyophilized to dryness. Each conjugate was further purified via reverse-phase high-performance liquid chromatography using an HP1100 HPLC system, a Varian DynaMax C18 semipreparative column, and an elution gradient of 85:15 to 40:60 H<sub>2</sub>O (0.1% TFA):MeCN (0.1% TFA) over 60 min.

ESI-MS: 478 [M-H]<sup>2+</sup>, 955 [M-2H]<sup>+</sup>

### 7.4.3.2: HANDLING OF RH-<sup>125</sup>I

Unless they are < 20 nm away from one's DNA, the Auger electrons emitted by <sup>125</sup>I are more or less harmless. The gamma rays and X-rays that the radionuclide also emits during its decay, however, are not. Therefore, considerable care was taken when working with the radiolabeled Rh-<sup>125</sup>I conjugate. Protective equipment (goggles, lab coat, nitrile gloves, and dosimeters) were worn at all times when handling the molecule. Further, when possible, all manipulations were conducted behind at least ¼" of protective lead sheets. Needless to say, all <sup>125</sup>I waste was sequestered from non-radioactive or <sup>32</sup>P waste. Both scintillation counter and Geiger counter surveys were performed rigorously after any experiments to ensure that no contamination had occurred. Finally, my thyroid was surveyed after every experiment by the Environmental Health and Safety Office to check for <sup>125</sup>I accumulation.

### 7.4.3.3: RH-<sup>125</sup>I DNA CLEAVAGE EXPERIMENTS

5 µL solutions of Rh-<sup>125</sup>I (60 nM, 1.25 µCi) were combined in 1.5 µL centrifuge tubes with equal volume solutions of 5'-<sup>32</sup>P-labeled oligonucleotides in a buffer of 40 mM NaCl, 10 mM NaPi, pH 7.1. Three concentrations of DNA were employed: 50 nM, 100 nM, and 150 nM. Four single stranded oligonucleoties were used to create duplexes with central C•G, C•A, or C•C sites. The forward strand DNA sequence was 5'-GAC CAG CTT ATC ATC CCT AGA TTA GCG-3'. The matched complement was 5'-CGC TTA TCT AGG GAT GAT AAG CTG GTC-3', the C•A mismatched complement was 5'-CGC TTA TCT AGG AAT GAT AAG CTG GTC-3', and the C•C mismatched sequence is 5'-CGC TTA TCT AGG CAT GAT AAG CTG GTC-3'. For each type of

duplex, experiments were run with each of the two strands labeled in order to check for double strand breaks.

After preparing the appropriate samples, the tubes were frozen at -80 °C for 7, 14, or 21 days. After incubation, the samples were thawed, diluted with denaturing loading dye, and electrophoresed on 20% denaturing polyacrylamide gels for 60–90 min at 90 W. Images of the gels were obtained via phosphorimager and quantified using ImageQuant software.

## 7.5: REFERENCES

1. Zeglis, B. M.; Pierre, V. C.; Barton, J. K. *Chemical Communications* **2007**, 4565–4579.
2. Zeglis, B. M.; Barton, J. K. *Nature Protocols* **2007**, 2 (2), 357–371.
3. Jackson, B. A.; Alekseyev, V. Y.; Barton, J. K. *Biochemistry* **1999**, 38 (15), 4655–4662.
4. Junicke, H.; Hart, J. R.; Kisko, J. L.; Glebov, O.; Kirsch, I. R.; Barton, J. K. *Proceedings of the National Academy of Sciences U. S. A.* **2003**, 100, 3737–3742.
5. Hart, J. R.; Johnson, M. D.; Barton, J. K. *Proceedings of the National Academy of Sciences of the United States of America* **2004**, 101 (39), 14040–14044.
6. Zeglis, B. M.; Boland, J. A.; Barton, J. K. *Journal of the American Chemical Society* **2008**, 130 (24), 7530–7531.
7. Zeglis, B. M.; Boland, J. A.; Barton, J. K. *Biochemistry* **2009**, 48 (5), 839–849.

8. Hart, J. R.; Glebov, O.; Ernst, R. J.; Kirsch, I. R.; Barton, J. K. *Proceedings of the National Academy of Sciences of the United States of America* **2006**, *103*, 15359–15363.
9. Ernst, R. J.; Song, H.; Barton, J. K. *Journal of the American Chemical Society* **2009**, *131* (6), 2359–2366.
10. Brunner, J.; Barton, J. K. *Biochemistry* **2006**, *45* (40), 12295–12302.
11. Lim, M. H.; Lau, I. H.; Barton, J. K. *Inorganic Chemistry* **2007**, *46*, 9528–9530.
12. Schatzschneider, U.; Barton, J. K. *Journal of the American Chemical Society* **2004**, *126* (28), 8630–8631.
13. Petitjean, A.; Barton, J. K. *Journal of the American Chemical Society* **2004**, *126* (45), 14728–14729.
14. Zeglis, B. M.; Barton, J. K. *Journal of the American Chemical Society* **2006**, *128* (17), 5654–5655.
15. Puckett, C. A.; Barton, J. K. *Journal of the American Chemical Society* **2007**, *129* (1), 46–47.
16. Puckett, C. A.; Barton, J. K. *Biochemistry* **2008**, *47* (45), 11711–11716.
17. Jackson, B. A.; Barton, J. K. *Journal of the American Chemical Society* **1997**, *119* (52), 12986–12987.
18. Jackson, B. A.; Barton, J. K. *Biochemistry* **2000**, *39* (20), 6176–6182.
19. Jackson, B. A.; Henling, L. M.; Barton, J. K. *Inorganic Chemistry* **1999**, *38* (26), 6218–6224.
20. Wong, E.; Giandomenico, C. M. *Chemical Reviews* **1999**, *99* (9), 2451–2466.

21. Rosenberg, B.; Vancamp, L.; Trosko, J. E.; Mansour, V. H. *Nature* **1969**, 222 (5191), 385–&.
22. Ahmad, S.; Isab, A. A.; Ali, S. *Transition Metal Chemistry* **2006**, 31 (8), 1003–1016.
23. Jamieson, E. R.; Lippard, S. J. *Chemical Reviews* **1999**, 99 (9), 2467–2498.
24. Alazard, R.; Germanier, M.; Johnson, N. P. *Mutation Research* **1982**, 93 (2), 327–337.
25. Ciccarelli, R. B.; Solomon, M. J.; Varshavsky, A.; Lippard, S. J. *Biochemistry* **1985**, 24 (26), 7533–7540.
26. Eastman, A. *Biochemistry* **1986**, 25 (13), 3912–3915.
27. Fichtingerschepman, A. M. J.; Vanderveer, J. L.; Denhartog, J. H. J.; Lohman, P. H. M.; Reedijk, J. *Biochemistry* **1985**, 24 (3), 707–713.
28. Pinto, A. L.; Lippard, S. J. *Proceedings of the National Academy of Sciences of the United States of America* **1985**, 82 (14), 4616–4619.
29. Salles, B.; Butour, J. L.; Lesca, C.; Macquet, J. P. *Biochemical and Biophysical Research Communications* **1983**, 112 (2), 555–563.
30. Zhai, X. Q.; Beckmann, H.; Jantzen, H. M.; Essigmann, J. M. *Biochemistry* **1998**, 37 (46), 16307–16315.
31. Pors, K.; Patterson, L. H. *Current Topics in Medicinal Chemistry* **2005**, 5 (12), 1133–1149.
32. Jiricny, J. *Embo Journal* **1998**, 17 (22), 6427–6436.
33. Aebi, S.; KurdiHaidar, B.; Gordon, R.; Cenni, B.; Zheng, H.; Fink, D.; Christen, R. D.; Boland, C. R.; Koi, M.; Fishel, R.; Howell, S. B. *Cancer Research* **1996**, 56 (13), 3087–3090.

34. Fink, D.; Aebi, S.; Howell, S. B. *Clinical Cancer Research* **1998**, *4* (1), 1–6.
35. Fink, D.; Nebel, S.; Aebi, S.; Nehme, A.; Howell, S. B. *International Journal of Oncology* **1997**, *11* (3), 539–542.
36. Fink, D.; Zheng, H.; Nebel, S.; Norris, P. S.; Aebi, S.; Lin, T. P.; Nehme, A.; Christen, R. D.; Haas, M.; MacLeod, C. L.; Howell, S. B. *Cancer Research* **1997**, *57* (10), 1841–1845.
37. Lin, X. J.; Howell, S. B. *Molecular Cancer Therapeutics* **2006**, *5* (5), 1239–1247.
38. Fuertes, M. A.; Alonso, C.; Perez, J. M. *Chemical Reviews* **2003**, *103* (3), 645–662.
39. Hay, R. W.; Miller, S. *Polyhedron* **1998**, *17* (13–14), 2337–2343.
40. Di Francesco, A. M.; Ruggiero, A.; Riccardi, R. *Cellular and Molecular Life Sciences* **2002**, *59* (11), 1914–1927.
41. Gelasco, A.; Lippard, S. J. *Biochemistry* **1998**, *37* (26), 9230–9239.
42. Laurent, J. P.; Morvan, B. *Journal of the Chemical Society–Dalton Transactions* **1993**, (14), 2141–2145.
43. Petitjean, A. A metallointercalator for the delivery and release of platinum based DNA drugs. California Institute of Technology, Pasadena, 2005.
44. Koi, M.; Umar, A.; Chauhan, D. P.; Cherian, S. P.; Carethers, J. M.; Kunkel, T. A.; Boland, C. R. *Cancer Research* **1994**, *54* (16), 4308–4312.
45. Volkert, W. A.; Hoffman, T. J. *Chemical Reviews* **1999**, *99*, 2269–2292.
46. Blower, P. J. *Transition Metal Chemistry* **1998**, *23* (1), 109–112.
47. Hoefnagel, C. A. *Anti–Cancer Drugs* **1991**, *2* (2), 107–132.
48. Larson, S. M. *Current Pharmaceutical Design* **2009**, *15* (9), 950–956.
49. Okarvi, S. M. *Cancer Treatment Reviews* **2008**, *34* (1), 13–26.

50. McDevitt, M. R.; Scheinberg, D. A. *Cell Death and Differentiation* **2002**, *9* (6), 593–594.
51. McDevitt, M. R.; Sgouros, G.; Finn, R. D.; Humm, J. L.; Jurcic, J. G.; Larson, S. M.; Scheinberg, D. A. *European Journal of Nuclear Medicine* **1998**, *25* (9), 1341–1351.
52. McDevitt, M. R.; Ma, D. S.; Lai, L. T.; Simon, J.; Borchardt, P.; Frank, R. K.; Wu, K.; Pellegrini, V.; Curcio, M. J.; Miederer, M.; Bander, N. H.; Scheinberg, D. A. *Science* **2001**, *294* (5546), 1537–1540.
53. Auger, P. *Comptes Rendus Hebdomadaires Des Seances De L Academie Des Sciences* **1928**, *186*, 758–760.
54. Watson, E. C.; Van den Akker, J. A. *Proceedings of the National Academy of Sciences of the United States of America* **1927**, *13*, 659–662.
55. Anderson, C. D. *Physical Review* **1930**, *35* (10), 1139–1145.
56. Buchegger, F.; Perillo-Adamer, F.; Dupertuis, Y. M.; Delaloye, A. B. *European Journal of Nuclear Medicine and Molecular Imaging* **2006**, *33* (11), 1352–1363.
57. O'Donoghue, J. A. *The Journal of Nuclear Medicine* **1996**, *37* (4), 3S–6S.
58. O'Donoghue, J. A.; Wheldon, T. E. *Physics in Medicine and Biology* **1996**, *41* (10), 1973–1992.
59. Cohen-Jonathan, E.; Bernhard, E. J.; McKenna, W. G. *Current Opinion in Chemical Biology* **1999**, *3* (1), 77–83.
60. Simons, J. *Accounts of Chemical Research* **2006**, *39*, 772–779.
61. Andersson, P.; Forssell-Aronsson, E.; Johanson, V.; Wangberg, B.; Nilsson, O.; Fjalling, M.; Ahlman, H. *Journal of Nuclear Medicine* **1996**, *37* (12), 2002–2006.
62. Yasui, L. S.; Hughes, A.; DeSombre, E. R. *Acta Oncologica* **1996**, *35* (7), 841–847.

63. Karamychev, V. N.; Panyutin, I. G.; Reed, M. W.; Neumann, R. D. *Antisense & Nucleic Acid Drug Development* **1997**, *7* (6), 549–557.
64. Panyutin, I. G.; Neumann, R. D. *Nucleic Acids Research* **1997**, *25* (4), 883–887.
65. Makrigiorgos, G. M.; Kassis, A. I.; Baranowskakortylewicz, J.; McElvany, K. D.; Welch, M. J.; Sastry, K. S. R.; Adelstein, S. J. *Radiation Research* **1989**, *118* (3), 532–544.
66. Howell, R. W.; Kassis, A. I.; Adelstein, S. J.; Rao, D. V.; Wright, H. A.; Hamm, R. N.; Turner, J. E.; Sastry, K. S. R. *Radiation Research* **1994**, *140* (1), 55–62.
67. Haefliger, P.; Agorastos, N.; Renard, A.; Giambonini–Brugnoli, G.; Marty, C.; Alberto, R. *Bioconjugate Chemistry* **2005**, *16* (3), 582–587.
68. Karamychev, V. N.; Reed, M. W.; Neumann, R. D.; Panyutin, I. G. *Acta Oncologica* **2000**, *39* (6), 687–692.
69. Kometani, T.; Watt, D. S.; Ji, T. *Tetrahedron Letters* **1985**, *26* (17), 2043–2046.